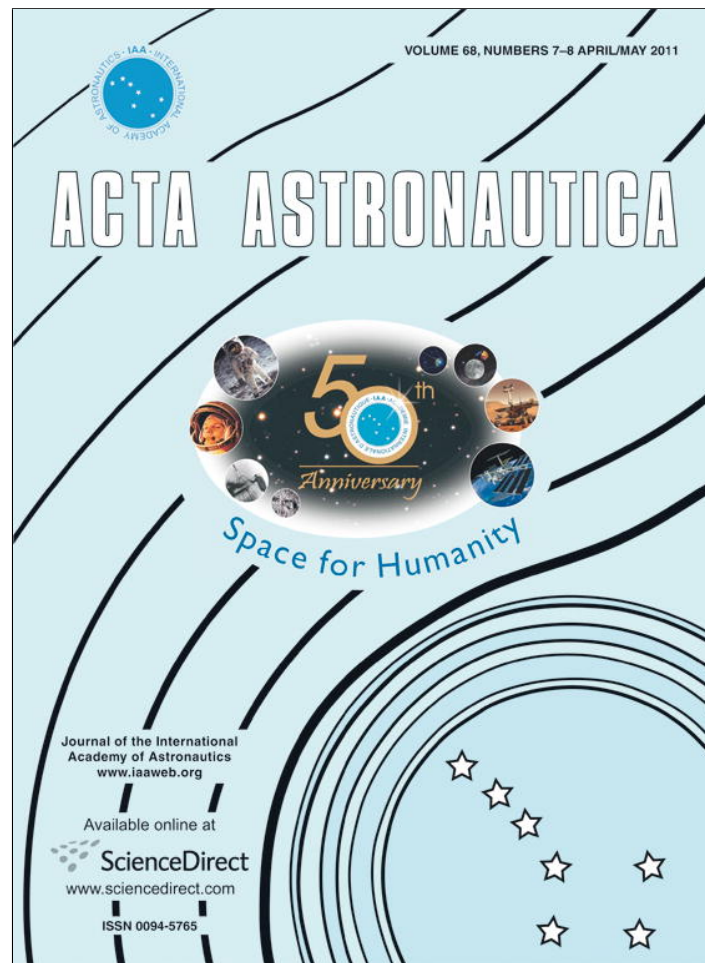


Provided for non-commercial research and education use.
Not for reproduction, distribution or commercial use.



This article appeared in a journal published by Elsevier. The attached copy is furnished to the author for internal non-commercial research and education use, including for instruction at the authors institution and sharing with colleagues.

Other uses, including reproduction and distribution, or selling or licensing copies, or posting to personal, institutional or third party websites are prohibited.

In most cases authors are permitted to post their version of the article (e.g. in Word or Tex form) to their personal website or institutional repository. Authors requiring further information regarding Elsevier's archiving and manuscript policies are encouraged to visit:

<http://www.elsevier.com/copyright>



Contents lists available at ScienceDirect

Acta Astronautica

journal homepage: www.elsevier.com/locate/actaastro

Structural health management technologies for inflatable/deployable structures: Integrating sensing and self-healing

Erik J. Brandon^{a,*}, Max Vozoff^{a,1}, Elizabeth A. Kolawa^a, George F. Studor^b, Frankel Lyons^b, Michael W. Keller^{c,2}, Brett Beiermann^c, Scott R. White^c, Nancy R. Sottos^c, Mark A. Curry^d, David L. Banks^d, Robert Brocato^e, Lisong Zhou^{f,3}, Soyoun Jung^{f,4}, Thomas N. Jackson^f, Kevin Champaigne^g

^a NASA Jet Propulsion Laboratory, California Institute of Technology, Pasadena, CA 91109, USA

^b NASA Johnson Space Center, Houston, TX 77058, USA

^c University of Illinois at Urbana-Champaign, Urbana, IL 61801-298, USA

^d Boeing Phantom Works, Seattle, WA 98124, USA

^e Sandia National Laboratories, Albuquerque, NM 87185, USA

^f Penn State University, University Park, PA 16802, USA

^g Invocon, Inc., Conroe, TX 77385, USA

ARTICLE INFO

Article history:

Received 29 April 2010

Accepted 17 August 2010

Available online 17 September 2010

Keywords:

Inflatable structures

Deployable structures

Distributed sensing

Structural health monitoring

Self-repairing materials

ABSTRACT

Inflatable/deployable structures are under consideration as habitats for future Lunar surface science operations. The use of non-traditional structural materials combined with the need to maintain a safe working environment for extended periods in a harsh environment has led to the consideration of an integrated structural health management system for future habitats, to ensure their integrity. This article describes recent efforts to develop prototype sensing technologies and new self-healing materials that address the unique requirements of habitats comprised mainly of soft goods. A new approach to detecting impact damage is discussed, using addressable flexible capacitive sensing elements and thin film electronics in a matrixed array. Also, the use of passive wireless sensor tags for distributed sensing is discussed, wherein the need for on-board power through batteries or hardwired interconnects is eliminated. Finally, the development of a novel, microencapsulated self-healing elastomer with applications for inflatable/deployable habitats is reviewed.

© 2010 Elsevier Ltd. All rights reserved.

* Corresponding author. Tel.: +1 8183932674.

E-mail addresses: erik.j.brandon@jpl.nasa.gov (E.J. Brandon), Max.Vozoff@spacex.com (M. Vozoff), Elizabeth.A.Kolawa@jpl.nasa.gov (E.A. Kolawa), george.f.studor@nasa.gov (G.F. Studor), frankel.lyons-1@nasa.gov (F. Lyons), mwkeller@utulsa.edu (M.W. Keller), bbeierm2@illinois.edu (B. Beiermann), swhite@uiuc.edu (S.R. White), n-sottos@uiuc.edu (N.R. Sottos), mark.a.curry@boeing.com (M.A. Curry), david.l.banks@boeing.com (D.L. Banks), rwbroca@sandia.gov (R. Brocato), Lisong_zhou@amat.com (L. Zhou), sxj001@uark.edu (S. Jung), tnj1@psu.edu (T.N. Jackson), champaigne@invocon.com (K. Champaigne).

¹ Present address: SpaceX, Hawthorne, CA 90250, USA.

² Present address: University of Tulsa, Department of Mechanical Engineering, Tulsa, OK 74104-3189, USA.

³ Present address: Applied Materials, Inc., Santa Clara, CA 95050, USA.

⁴ Present address: University of Arkansas, Fayetteville, AR 72701, USA.

1. Introduction and motivation for work

Recent efforts have focused on the development of new technologies for returning humans to the Lunar surface [1]. Whereas previous missions involved two crew members conducting surface operations over a limited time frame (1–3 days), future exploration plans call for the emplacement of larger crews of scientists on the Moon for one month or longer. Achieving extended operations and maintaining a sustained presence on the Moon will require structures for housing the crew much larger than the Apollo-era Lunar Module.

Previous design trade studies conducted by the National Aeronautics and Space Administration (NASA), by academia

and by industry have indicated that placing a habitat on the Lunar surface that is large enough to support both the physical and psychological needs of a crew will be challenging to achieve using pre-integrated, rigid modules, the approach used for constructing the International Space Station (ISS) [2,3]. Longer term Lunar exploration plans focus on the construction of Lunar habitats using materials processed from the Lunar regolith, but would be implemented much farther in the future due the logistics challenges of processing *in situ* resources.

A middle course between these two extreme habitat configurations is based on the use of inflatable structures (Fig. 1), which would be deployed on the Lunar surface [4–20]. Inflatable/deployable structures employ structural members comprised of soft goods such as fabrics, foams and elastomeric polymers, in place of traditional engineering materials such as metal alloys and rigid composites. The structure is initially stowed in a folded configuration, allowing the payload to be accommodated to a variety of launch vehicle shrouds and thus offering more flexible launch manifests. Once in place, the structures are deployed through pressurization and mechanical actuation, with rigidity maintained either through continual repressurization of the structure or through various rigidization mechanisms such as ultraviolet (UV) or thermal curing of polymer materials. Although there are many different specific variations in inflatable technology, all inflatable structures share these broad design features.

Inflatable/deployable structures are thus attractive as surface habitats for four key reasons:

- **High volume-to-mass ratio:** The livable habitat volume that can be delivered to the Lunar surface per unit mass of payload can be maximized. It has been determined that 120 m³ per crew member will likely be needed for longer-duration stays, which is difficult to achieve for larger crews using rigid, pre-integrated modules [10].
- **High packaging efficiency:** Inflatable/deployable structures provide for a more flexible launch manifest,

whereby the structure can be designed more efficiently around the launch vehicle.

- **Minimal need for on-site construction materials:** With these unique habitats, virtually all of the assembly mechanism is inherent to the structure, although Lunar regolith may be used in the long term to provide radiation shielding, micrometeoroid protection, and to dampen thermal variations [3].
- **Fewer secondary radiation effects:** Use of soft goods reduces the destructive effects of secondary ionizing particles, commonly seen with metallic structural materials.

Although other factors such as lower cost are cited as favorable attributes, these four specific characteristics are unique to inflatable/deployable structures (versus pre-integrated modules or fully *in-situ* derived habitats).

Consideration of inflatable/deployable habitats, particularly for the Lunar surface, reaches back to the early 1960s as the first United States human Lunar exploration program progressed [4]. The next significant developments in this area involved a series of concept studies in support of the United States Space Exploration Initiative in 1989 [2], and again in the mid-1990s initially in the form of the Expandable Lunar Lander concept [6]. This led to the Transit Habitation projects [6] at NASA's Johnson Space Center in 2000 [8,9]. The technology developed by this project has since been licensed by Bigelow Aerospace for implementation as a part of a commercial enterprise, ultimately aimed at the space tourism market [5]. Throughout these forty years of development, the technology has progressed from conceptual designs to hardware of increasing maturity, culminating in the launch into low Earth Orbit of the first space-based inflatable habitat (built by Bigelow Aerospace), the Genesis module, in July 2006.

As for all human-rated space vehicles, the need to maintain the safety of the crew is paramount. One approach to addressing this need involves the implementation of an integrated structural health management system (SHMS), to detect and alert the crew to unforeseen

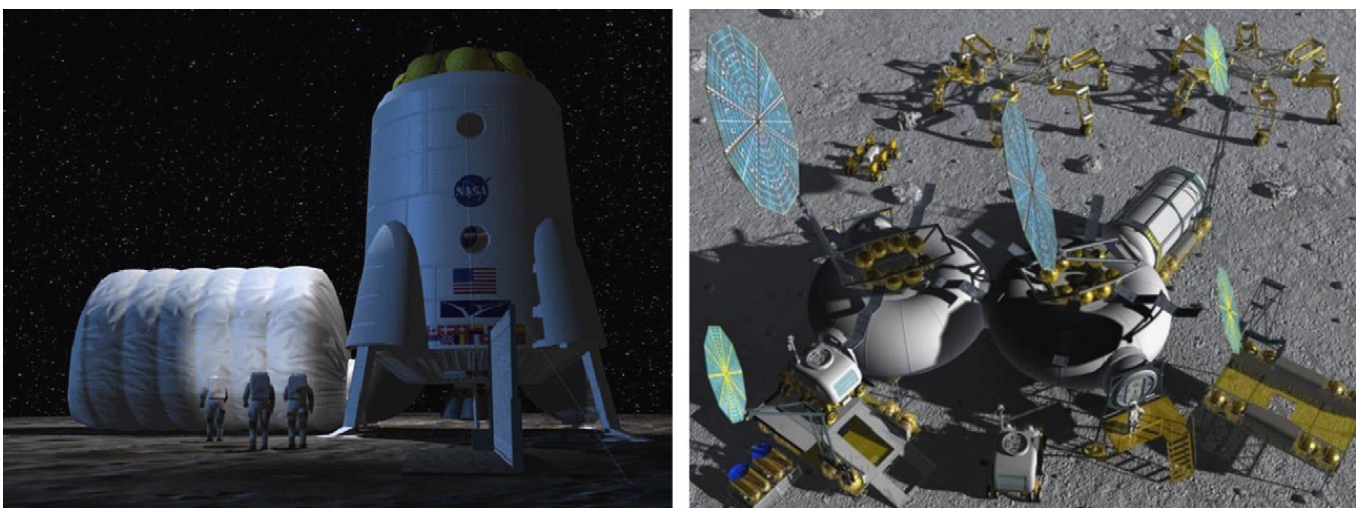


Fig. 1. Conceptual views of cylindrical and toroidal inflatable habitats on the Lunar surface.

damage and adverse structural conditions. Given the unique design and nature of the materials used in inflatable/deployable structures, it is anticipated these habitats will have unique health monitoring needs that call for new monitoring techniques. Driven by this need, NASA recently initiated development efforts for structural health management technologies specifically aimed at meeting the unique requirements of inflatable habitats.

Under the auspices of NASA and the National Science Foundation, a terrestrial inflatable habitat was monitored at the McMurdo Complex in Antarctica. This prototype structure was manually deployed in the field by a team of technicians, and served as a testbed for the characterization of discrete point sensors attached to the structure. Future Lunar habitats will be launched in advance of the arrival of humans, however, and will need to be packed in a highly efficient container, deployed remotely with no human intervention and monitored for proper deployment. Highly capable habitats of this class are anticipated to feature integrated sensors in a distributed network architecture. Long term NASA goals include developing technologies for sensing and monitoring, as well as for adapting the structure autonomously in response to sensor input, to mitigate adverse conditions when possible.

Section 2 of this article discusses general needs for health monitoring in inflatable/deployable structures based on the results of a preliminary needs analysis with input provided by various habitat stakeholders. Section 3 then discusses general approaches to a health management system, in the context of the unique requirements imposed by inflatable/deployable habitats. Section 4 then reviews initial results from recent efforts aimed to develop suitable sensing and health monitoring technologies.

As indicated, there is also a desire to embed adaptive capabilities into the structure, to respond autonomously to information provided by integrated sensing technologies. Numerous adaptive capabilities may be integrated within such a structure that would increase crew safety and reduce the amount of maintenance time. Some of the capabilities under consideration include coatings which can vary their emissivity signatures to control temperature and actuators based on piezoelectric materials, shape memory alloys or magnetostrictive materials for modifying and maintaining the proper shape of the habitat, following deployment. However, the key concern for managing the habitat structural health regards mitigating impact damage. Therefore, the development of self-healing materials designed specifically for habitat structures is discussed in Section 5.

2. Specific habitat structural health management needs

There is little flight heritage to date to provide feedback on the long term performance of space-borne inflatable habitat structures. The highest fidelity NASA hardware to date is represented by the Transit Habitat, or TransHab architecture depicted in Fig. 2.

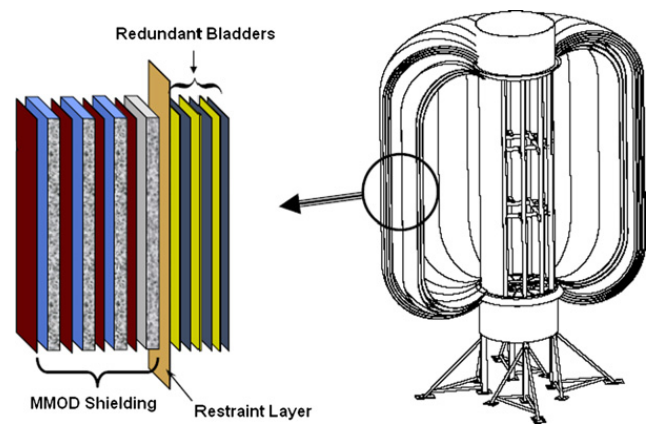


Fig. 2. Cross-sectional schematic view of the Transit Habitat (TransHab) inflatable structure, highlighting the micrometeoroid and orbital debris shielding, restraint layer and redundant bladders.

Although the final Lunar habitats have yet to be designed, most current inflatable habitat designs are based on this heritage technology and will share many common features. Thus, the architecture of the TransHab provides a representative structure and conceptual framework to contemplate technologies that would be needed for structural health management [6–10]. As seen in Fig. 2, it is a hybrid structure featuring a rigid inner core and inflatable outer shell. This outer shell is comprised of multiple layers, each providing key functions. This includes multiple redundant bladder layers for containing the breathable volume of atmosphere, a woven Kevlar load-bearing restraint layer and a multi-shock micrometeoroid and orbital debris (MMOD) shield comprised of alternating layers of Kevlar and polyurethane foam. Depending on the specific mission, other functional layers may be incorporated into the structure, including blanketing for thermal control and atomic oxygen protection. Several journal articles and conference proceedings provide design details regarding specific materials used [6–10].

Given that no design or specific plan for a Lunar habitat currently exists, it is difficult to derive detailed requirements for a health management system. Therefore, the focus of efforts described here was to identify common themes, trends, or elements that have shaped the thinking of inflatable/deployable habitat design to date, and to use this knowledge as a basis for developing high-level goals and targets that could provide a framework for the development of appropriate structural health management technologies. This information was derived through a detailed review of the published literature as well as discussions with habitat structural engineers and architects, materials scientists, astronauts and flight operations personnel.

Monitoring of impact damage upon the structure, to alert the crew as to their location and severity, is considered a top priority. This includes impacts by hypervelocity particles (such as micrometeoroids) as well as slow moving impacts by humans or vehicles operating inside or outside the periphery of the habitat. The health monitoring system should provide for identification of the event time, location of the impact, depth of penetration

and the extent of the resulting damage. The crew should be immediately notified if urgent action is required. This need applies equally to orbiting habitats and surface habitats. This information allows accurate assessment of mission impact and habitat lifetime, prioritization of any maintenance or repair, and ensures that the crew is appropriately equipped for any required extravehicular activity (EVA) for repairs. Recent monitoring of the Lunar surface indicates regular impacts by sporadic and shower meteoroids [21]. It was estimated that 2–3 sporadic meteor impacts occur per hour, with masses of 1 kg (large enough to be observed from Earth). These recent data represent only the readily observable impacts, and there are presumably many more smaller particles than this that regularly reach the Lunar surface and may pose a threat to a habitat. Related to the need for measuring impacts is leak detection, which may or may not be caused by impacts but could aid in the localization of damage causing impacts. As indicated earlier, a long term goal is to couple an impact damage detection system with a self-healing capability.

Another health monitoring need is the assessment of structural strain around various interfaces, particularly where soft and hard materials meet. Most proposed habitat designs include both flexible and rigid components. Flexible components include bladder membranes and woven restraint layers. Rigid components include metallic bulkheads, air locks and windows. The interface between these soft and hard materials and the abrupt transition in structural properties are difficult to model, and empirical measurements from embedded sensors, on either side of the interface, will be important to validating specific designs. Some habitat designs feature windows, and monitoring the integrity of window seals is considered critical.

Finally, there are other structural health monitoring needs that are not considered vital to ensuring crew safety during long duration missions, but that may provide added benefits to ensure overall mission success. For example, it is envisioned that habitats will be launched to the surface and deployed prior to the arrival of humans. Thus, monitoring deployment dynamics to ensure proper inflation and determining the ultimate dimensions and shape of the habitat are also considered possible features for incorporation into an SHMS. This will enable ground crews to determine whether or not the habitat is in a suitable configuration prior to sending humans to occupy the structure. Data from an embedded network of sensors may be effectively combined with visual imagery from on-board video cameras to convey this type of information. Again, adaptive capabilities based on integrated actuators may eventually play a role, allowing the structural shape or configuration to be modified as needed, if problems occur during the deployment process.

3. Challenges and approaches to embedding health management technologies

The previous section provided an overview of the key high level structural health management needs for

inflatable/deployable habitat structures. Selecting appropriate technologies and architectures to meet these needs is made difficult when considering traditional structural health monitoring solutions such as bonded strain gages and fiber optic sensors. This is due to the fact that most aerospace and aeronautics structural health monitoring technologies are geared toward rigid structures where integration and mounting of sensors is not a significant issue, and wires and cabling for data communications and power distribution are easier to implement alongside related wiring for the myriad existing avionics subsystems.

Implementing such approaches in an inflatable or deployable habitat requires any wires or fiber optics to be pre-positioned before packing (and maintaining integrity when folded and during deployment), or else be installed after deployment. The latter makes the deployment sequence more complex and labor-intensive. It also means sensor data is unavailable until these wires are installed, precluding these sensors from monitoring the deployment process (a key potential benefit of using an SHMS). Providing power to, and obtaining data from, the large numbers of point sensors in distributed locations that will be required to provide adequate health data is also a design challenge.

One means to circumvent these problems is to use distributed networks of ultra-low-power or even no-power point sensors (such as strain gages and acoustic leak detectors) in conjunction with wireless communications to alleviate or even eliminate the cabling problems. The complexity associated with cabling on recent space vehicles and structures (as measured in harness drawings, cable and connector installations and launch weight penalties) continues to increase with time. These issues will be multiplied in an inflatable habitat, where stowage and deployment issues must also be considered. Wireless solutions limit the number of connectors and penetrations required, thus offering design flexibility and a means to reduce the complexity of integrating an SHMS.

For example, wireless devices have recently been installed for wing lead edge impact monitoring on the Space Shuttle as a retrofit option, eliminating time consuming requirements for cable installation and drawing modifications. Similarly, a network of wireless temperature sensors was recently installed prior to launch on an ISS module within just two months after the need for additional instrumentation was identified. Similar advantages can be envisioned for Lunar habitat applications. In order to minimize the complexity of integrating new sensors late in the design cycle of a Lunar habitat, sufficient infrastructure such as wireless interfaces to standard data busses will need to be designed into the habitat.

For distributed sensor systems, tradeoffs regarding power distribution, generation and storage must also be considered. Traditional wired electrical power distribution can become a significant portion of a vehicle or habitat total mass, due to the large conductor sizes, connectors, cable clamps, power-conversion electronics and fault-detection circuitry. When highly distributed sensing by low-power nodes is employed, alternative

power concepts must then be considered. For example, by distributing low-voltage power to each node, the need for power-conversion electronics at each node can be eliminated. By employing local energy storage (either battery or capacitor based) at a remote node, the instantaneous current requirements for particular power supplies can be limited, thereby reducing the size of the cabling and fault-detection circuitry.

Power scavenging concepts may also be considered for low-power devices, although these concepts are difficult to implement for highly embedded sensors which are shielded from light (for photovoltaic harvesting) and dampened from vibrations by soft materials (for kinetic energy harvesting). Concepts for power generation by means of thermal differentials may provide limited means for very low power harvesting within habitat structures. A more straightforward approach, however, is to use remote power distribution through radio-frequency (RF) sources. Although the total system efficiency is generally rather low, this type of system can either utilize temporary energy (e.g., through batteries) or simply operate when sufficient instantaneous power has been harvested and is available.

There are issues, however, in mounting these type of electronics in an inflatable/deployable structure such that they remain in place during and after deployment, and do not interfere with the deployment process in any way. The structure itself can also be impacted by the inclusion of the sensors, through stress concentration at the point of attachment or through the adhesives or related joining technologies which may alter the materials properties of the underlying substrate. One solution to help circumvent these issues is to use a multifunctional materials approach in which inherently flexible sensors and electronics are integrated or embedded between layers, along with the necessary flexible electronics for data acquisition and processing [22–34].

Implementing data and power interconnects for flexible electronics will require unique architectures such as addressable matrix arrays that reduce the amount of wiring needed by sharing of common buses by multiple sensor patches. Consideration of a flexible electronics approach is made possible by developments over the last twenty years in the design and processing of amorphous and thin film semiconductor materials and devices. These technologies include methods for manufacturing electronics directly onto large area flexible substrates for displays, sensing and even limited data processing.

As a measure of progress in this area, industrial efforts in the field of flexible electronics are now rapidly accelerating and moving away from demonstration and prototyping of small scale hardware to issues of larger area manufacturing and long term reliability of devices [24–26]. Flexible electronics are now under consideration for a wide range of applications where large area coverage and mechanical flexibility are key design drivers. This includes applications ranging from medical imaging to space-borne radar [24]. These same approaches are under consideration by NASA for integration with inflatable habitats for structural health sensing. Recently, the first radiation testing of flexible organic transistors

was completed, to evaluate the suitability of these materials and devices for space applications [32]. The key challenge in implementing such an approach is that sensors and associated electronics must be compatible with the underlying substrate and survive the fabrication processes, stowing, launch, deployment and operations.

Thus, to implement a structural health management system, questions of how best to embed sensors that can undergo stowage and deployment, particularly in the context of wiring for power and data acquisition, must be answered. Solutions for health monitoring in inflatable/deployable habitats will likely feature a combination of wireless point sensors and embedded flexible sensors. Flexible sensing technologies are well suited for “blanket coverage” approaches that are needed for situations such as impact damage detection or monitoring of strain over large areas. Wireless point sensors, however, may be more useful for applications where complete area coverage is not required, such as impact/strike detection (via accelerometers) or leak detection (using ultrasonic and acoustic transducers).

4. Integrated sensing

The needs analysis outlined in Section 2 identified the ability to detect in real time impacts upon the habitat (particularly those leading to penetration and damage of the structure) as a critical capability for any structural health monitoring system implemented in inflatable/deployable structures. The requirements for an impact detection system are to spatially locate damage and rapidly determine the size and depth of the penetration in real time, so the crew can determine the proper course of action. One approach to meet this requirement is to implement a “blanket” sensor array, in which critical surfaces are covered with sensors capable of detecting impacts. Numerous previous technologies have been used for detecting impacts on spacecraft, none of which are suitable for inflatable habitats [35–37]. To facilitate integration with the structure and minimize interference with the deployment process, the sensor technology must be minimally invasive, and preferably thin and flexible. As part of the sensor development program reported herein, two different approaches to flexible, blanket detection were evaluated. One approach is based on embedded flexible inductors, for integration with multi-layer thermal blanketing (discussed in Ref. [38]). The other sensing technology was designed for incorporation into a variety of inflatable/deployable habitat structural materials and is based on embedded capacitors (discussed in the following section).

4.1. Flexible impact detection using capacitive sensor arrays

4.1.1. Theory of operation

The capacitive impact damage sensor system is based on an array of individual capacitors, fabricated using polyimide-based flexible circuit technology. During operation, an applied voltage across each of these sensors is continually monitored. Any changes due to impact

damage are manifested as changes in capacitance, due to the change in area of the dielectric layer.

The capacitive sensors are arrayed in an addressable matrix monitored in real time, to provide spatial and temporal information regarding impacts. When the capacitor is damaged by a penetration, the effective capacitance of the sensor is modified, and this change can be monitored to convey damage information. Each unit cell of the array utilizes a shielded capacitor geometry, comprised of a metal/dielectric/metal/dielectric/metal multi-layer (constructed from copper metalized 75 μm thick polyimide substrate) in which the ground planes are shorted. The use of a shielded structure with ground planes provides a degree of immunity from external electric fields. These sensors are depicted schematically in Figs. 3 and 4.

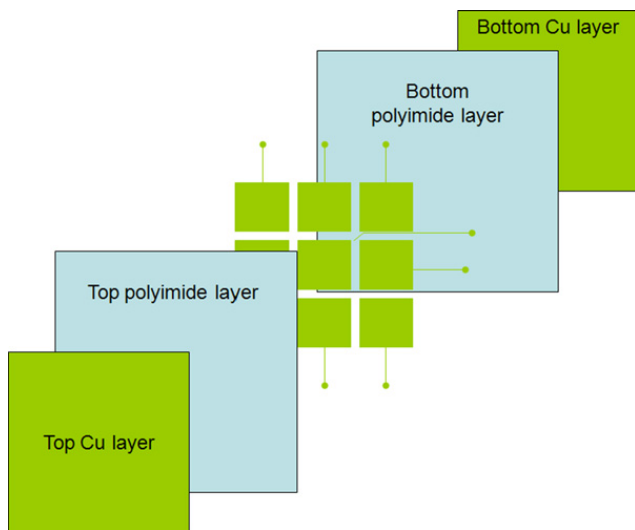


Fig. 3. Exploded schematic view of capacitive sensor array, depicting the top and bottom Cu electrodes/shields and the inner dielectric and electrode patches.

To monitor the array, a voltage is applied to each capacitor. The change in voltage (ΔV) during charging is dictated by the charging current, the thickness of the dielectric, the dielectric constant and the area of the plates:

$$\Delta V = \frac{i_c d \Delta t}{2 \epsilon_r \epsilon_0 A} \quad (1)$$

where i_c is the charging current, d the dielectric layer thickness, Δt the charging time, ϵ_r the relative dielectric permittivity, ϵ_0 the vacuum permittivity and A the capacitor area. If a capacitor is punctured, the effective area (A) will be modified, thus changing the final voltage reached after a fixed charging time. This change in voltage (or alternatively change in charging time) can be detected using appropriate readout electronics. By determining which specific capacitor in the array is affected, the location of the damage can be determined within the resolution of the size and spacing of the individual capacitive sensors. By determining the magnitude of change in capacitance (which is related to the change in area induced by the damage) it may be possible to develop an algorithm to correlate the magnitude of change in capacitance with the degree of damage.

With the capacitor charging current given below as

$$i_c = C \frac{dV}{dt} \quad (2)$$

where dV/dt is the change in voltage with time, it is apparent that if the charging current is held constant, the voltage change is linear with time. Therefore, the approach for detecting damage in the proof-of-concept array was to apply a current and measure the resulting voltage at the end of time t to yield the change in capacitance C before and after simulated damage.

4.1.2. Hypervelocity impact testing of prototype capacitive sensing elements

To determine the feasibility of using flexible capacitors as a damage detection sensing element, the first step was

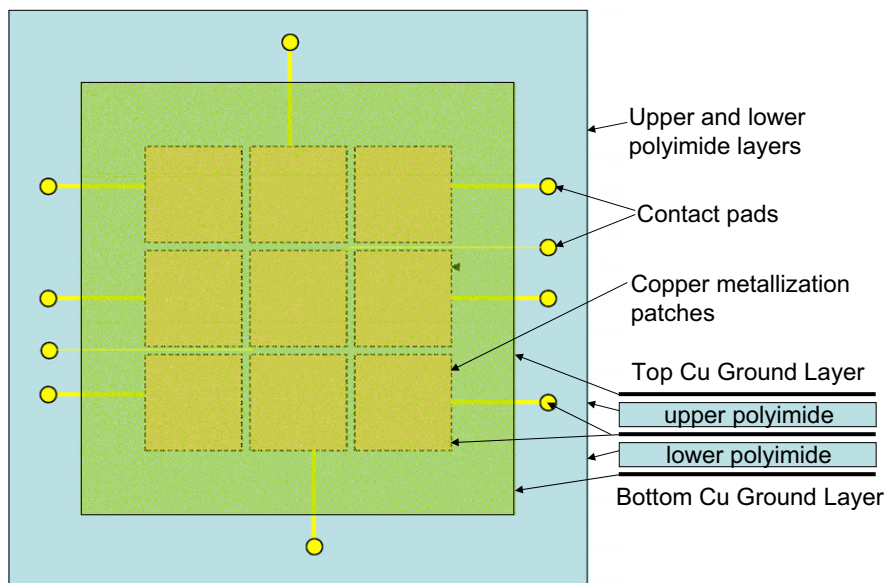


Fig. 4. Detailed schematic view of capacitive sensor array. The dimensions of the full sensor array are approximately 15×15 cm.

to determine typical damage patterns on prototype sensing elements that may be encountered upon impact by a representative hypervelocity particle, and to correlate these damage pattern with measured changes in capacitance. A series of hypervelocity impact tests were thus conducted at the NASA White Sand Test Facility in White Sands, New Mexico.

Aluminum plates were used to secure the multiple non-metallic layers in the correct configuration, with threaded rods used to properly space the multiple plates, as shown in Fig. 5.

The test article featured multiple layers of habitat materials in a configuration representative of a multi-layer habitat wall, including fiberglass-7781 (five layers), Kevlar 710 (five layers), capacitive sensors (three layers) and a 0.508 mm thick 6061-T6 aluminum witness plate (WP). An example target layout depicting the cross-sectional lay-up of these stacks is illustrated in Fig. 6.

The capacitance of each sensor was measured prior to impact testing. In each stack were three capacitive sensors, one placed near the outer surface, one near the middle and one near the rear of the stack. This arrangement allowed for assessing the damage to each sensor as a function of depth. Either a 1.0 or 2.8 mm aluminum sphere was used as the impacting particle at a velocity

of approximately 7 km/s. Damage was then assessed visually, and change in capacitance measured using a standard LCR meter.

Representative visual images and electrical sensor data are depicted in Figs. 7 and 8, with further data given in Table 1. As seen in Fig. 7, a 1.0 mm particle fired at 6.9 km/s creates a well defined, nearly round puncture in the top sensor approximately 4.1 mm in diameter, but the middle and back two sensors are not breached. The change in capacitance is enumerated in Table 1, with the 3.5% decrease in capacitance indicating the damage in the top layer. In this case, a fully configured system using this sensor technology integrated in an actual habitat structure would have quickly confirmed damage to the outer layer, indicating no breach of the inner layers.

This damage profile as a function of depth is contrasted with that observed for a second set of tests depicted in Fig. 8, indicating damage from a 2.8 mm particle fired at 7.27 km/s. In this case, the depth profile indicates a well defined puncture in the top layer (approximately 6 mm in diameter), a larger puncture (22–25 mm in diameter) accompanied by tearing of the middle layer, with an impact crater in the back sensor with no accompanying penetration. Measured capacitance data is given in Table 1. The top sensor registered as a short, thus signaling damage with no means to assess the magnitude of the damage. The middle sensor registered a 10% decrease in capacitance, whereas the back layer registered an increase of 6% (due to compression of the dielectric material and an effective decrease in dielectric thickness).

In an actual array integrated within a habitat structure, the multi-layers would have indicated a breach of the two outer layers, with some compromise of the back layer due to the more energetic particle. In a multi-layer structure such as an inflatable habitat where different complex multi-layers play a variety of roles from thermal blanketing to containing the breathable atmosphere, this type of quick insight into the extent of damage between layers can provide invaluable data to a crew making rapid decisions as to whether to seal a leaking habitat module and enter a safer one or if there is no immediate danger to the crew, complete repairs at a later time.

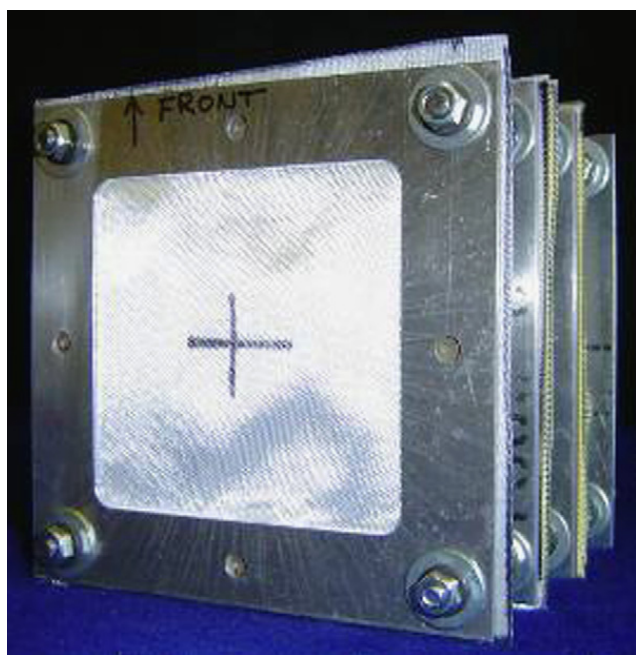


Fig. 5. Capacitive impact sensor test article, including the aluminum frame (15.2 cm × 15.2 cm) used to fix the representative habitat materials and sensors in place during testing.

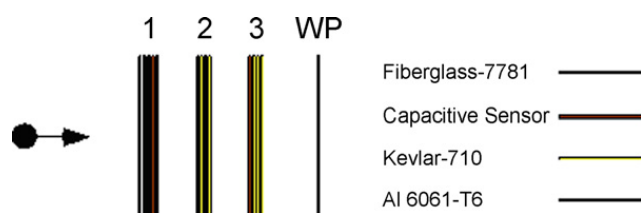


Fig. 6. Example target layout, featuring a multi-layer of fiberglass and Kevlar, interspersed with capacitive sensing elements.

4.2. Sensor readout and integrated flexible electronics

4.2.1. Prototype sensor array using discrete electronics

The blanket distributed sensor approach will ultimately be enabled using an addressable array architecture, whereby sensor elements are isolated and individually read, analogous to large area display technology. In place of picture elements or “pixels,” however, the addressable elements are sensors. By employing shared data acquisition lines, the need to individually provide each sensor with its own power and data connections is eliminated, thereby reducing the amount of interconnect wiring required.

Following the initial evaluation of individual sensor elements in a hypervelocity environment and correlation of damage patterns with capacitance changes, efforts focused on developing appropriate means for eventually

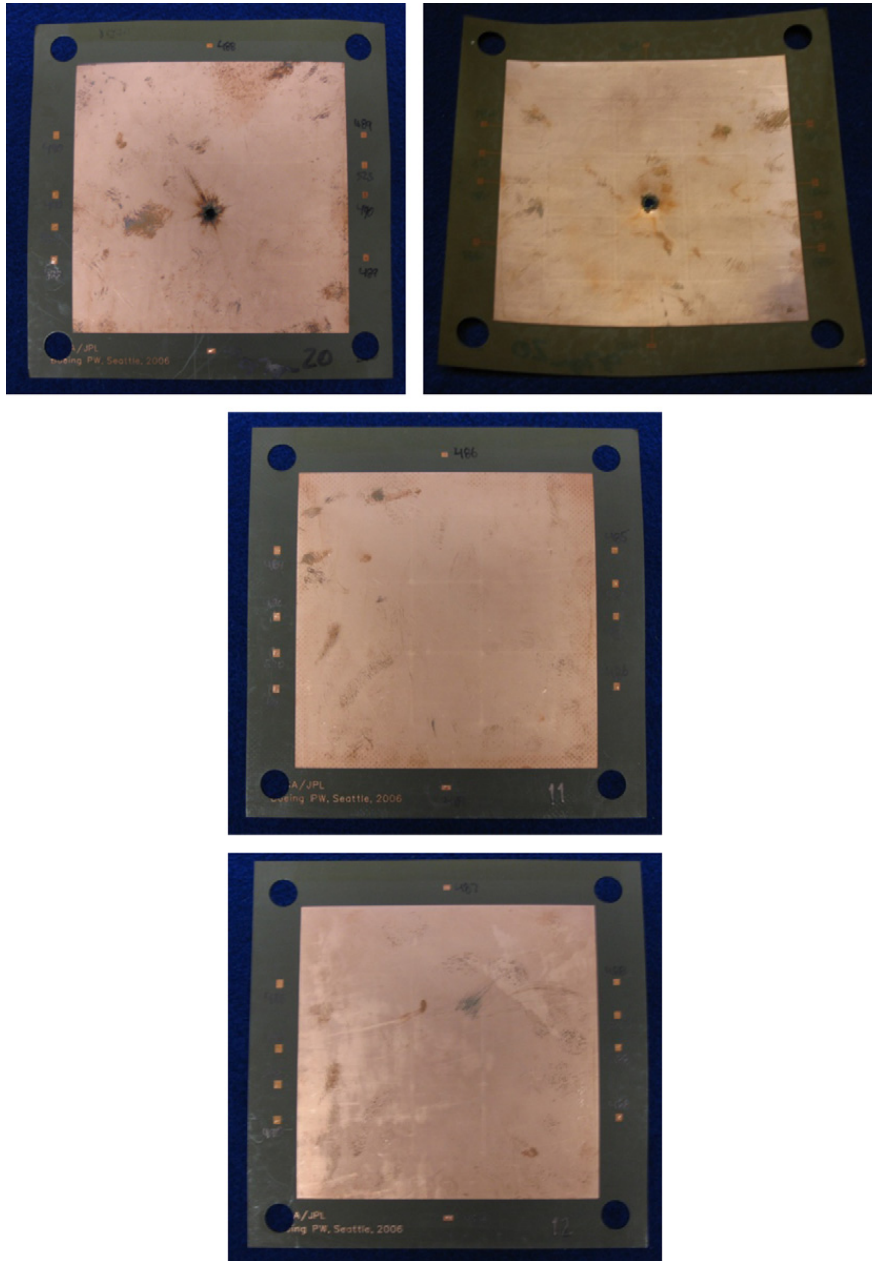


Fig. 7. Capacitive sensors impacted with a 1.0 mm projectile at 6.9 km/s. From top to bottom is the top layer (front and back views), middle layer (front view) and back layer (front view).

reading fully integrated arrays. A first generation readout system was developed using discrete electronic parts, interfaced to a 2×2 prototype sensor array (Fig. 9).

A block diagram of the data acquisition electronics is depicted in Fig. 10. A FLASH programmable PIC16F84 microcontroller running at 8 MHz and programmed in C serves as the array controller. The controller energizes a row at 5 V and triggers a current source charging of that row for 2 μ s. A single NMOS transistor is connected via its gate to each capacitor as it charges, with the source of the transistor connected to the sense line. The transistor at each unit cell acts as a buffer to isolate the patch from the rest of the array. The DC voltage is then read across a resistor attached to each capacitor patch, using an analog-to-digital (A/D) converter. The A/D interface and row/column scanning are controlled by the microcontroller, which continuously scans

the array and outputs the capacitor charge on the serial port as a 'SYNC' word followed by four raw data values. Voltage changes are read via a serial link by a microcomputer using a MATLAB program.

To test the readout capabilities of the sensors and circuitry, damage to the array was simulated by drilling 1 and 2 mm holes into two different capacitor sensors (depicted in Fig. 9). Operation of the electronics was confirmed by monitoring the change in the charging voltage when a 1 mm hole is introduced (by 0.8%) and a 2 mm hole (by 1.6%). No change in charging voltage was observed for the remaining undamaged sensors.

4.2.2. Flexible electronics for array sensing

The next step in the development of habitat impact sensing is to integrate the transistor patch switches with

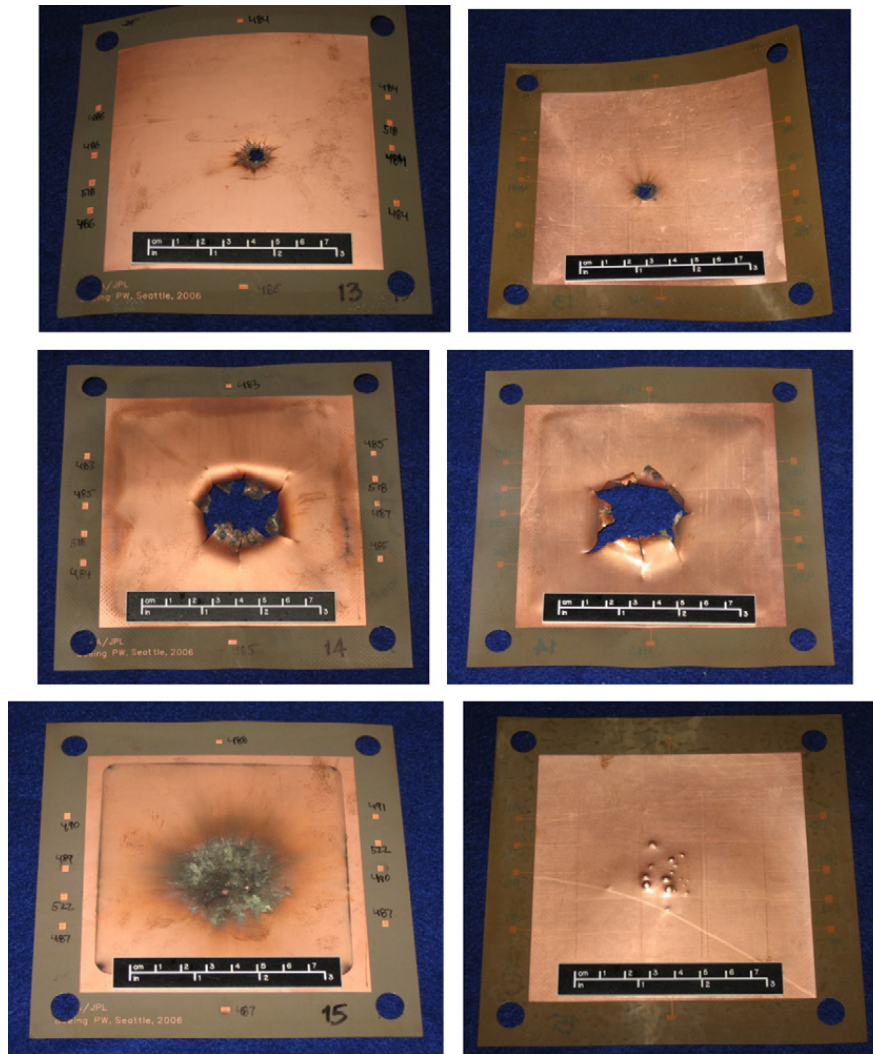


Fig. 8. Impact damage on capacitive sensors located at the top, middle and back layers of the stack (front and back views in each case) following impact from a 2.8 mm particle at 7.27 km/s.

Table 1
Capacitive sensor impact data.

Projectile size (mm)	Velocity (km/s)	Percent change in capacitance vs. baseline value (approximate hole diameter in parentheses)		
		Top sensor	Middle sensor	Back sensor
1.0	6.9	−3.5% (4.1 mm)	0	0
2.8	7.27	Shorted (6 mm)	−10% (22–25 mm)	+6%

the sensor array, within the same substrate. The ability to incorporate flexible thin film transistor technology (TFT) directly integrated with the substrate obviates the need to attach discrete transistor switches and opens the possibility to manufacture all of the sensors and electronics directly onto the structural materials using large area, roll-to-roll processing. This may include TFTs for use as switches, as well as alternative thin film materials that expands the range of sensor types beyond patterned copper/polyimide capacitors. Furthermore, the use of a robust flexible TFT technology to incorporate large arrays of blanket sensors facilitates deployment and stowage of

the structure (versus discrete electronics that are attached to the surface).

As discussed in Section 3, the concept of using large distributed arrays of sensors has gained currency in recent years as the technology focus has shifted from the production of small scale test coupons to the development of larger scale manufacturing capabilities [24–26]. This shift has been driven by the development of new materials, deposition methods and lithographic equipment by display manufacturers, and supported by the development of public/private consortia such as The Center for Advanced Microelectronics Manufacturing at

Binghamton University and the Flexible Display Center at Arizona State University. Many of these efforts have focused on the fabrication of electronics and sensors on arbitrarily sized flexible substrates, the same types of substrates that will be used to fabricate the impact array sensors.

The goal of the current effort was to investigate the migration of discrete, attached electronics outlined in the previous section to thin film integrated devices. The longer term goal is to develop a fully integrated system, featuring TFTs to isolate and readout capacitive arrays, along with thin film strain sensors and temperature sensors. In line with related industrial and academic efforts, the current work in developing flexible compo-

nents and devices is driven by a range of industrial interests from large area medical imaging to developing electronic “skin” that could be incorporated into robotic appendages [22–34]. As a technology demonstration, a prototype flexible arrayed matrix was fabricated using thin film strain sensors as the sensor node combined with flexible thin film transistors switches for selection of individual sensors *on the same substrate*. The thin processing technologies and readout approaches have been developed at Penn State University, and focus on the use of integrated strain gages which are of particular interest for health monitoring in inflatable/deployable habitats. As indicated in Section 2, there is a need to monitor the interfaces between hard and soft materials. Strain gages for monitoring rigid materials are well known, however significant challenges exist in interfacing traditional strain gages to thin, low modulus structural materials (typical of those found in habitats) and accurately transmitting strains to the strain gage (as in a foil based strain gage mounted using an epoxy). By directly depositing a strain gage on the underlying substrate under test, strain of the underlying structure is accurately coupled to the gage. If addressable arrays can be successfully integrated (similar to capacitive impact sensors), strain can be mapped out over large areas of the substrate. This approach could be used to detect issues or changes with, for example, the bladder layers, where the long term structural integrity is critical. Distributed strain gages could also be used to monitor the overall state of the structure before, during and after deployment.

A typical example of a single addressable array patch is shown in Fig. 11. The sensor features four microcrystalline silicon resistors arranged as a Wheatstone bridge. The width of each resistor is 18 μm and the length is approximately 200 μm.

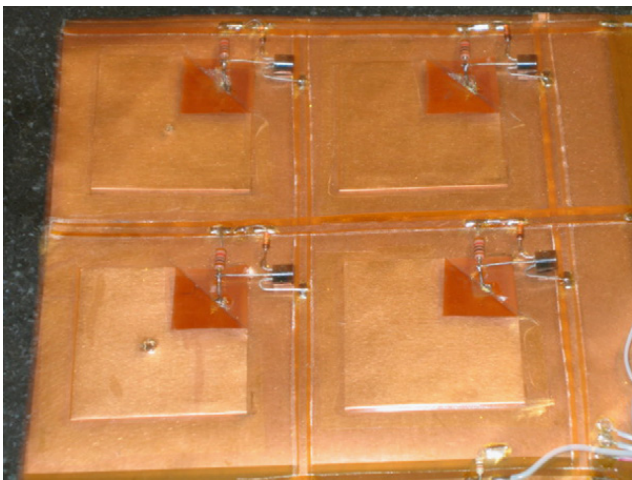


Fig. 9. 2 × 2 array of capacitive sensors, mounted for integration with breadboard data acquisition electronics. A 1 mm hole is drilled into the upper left sensor element and a 2 mm hole in the lower left sensor element, to simulate impact damage.

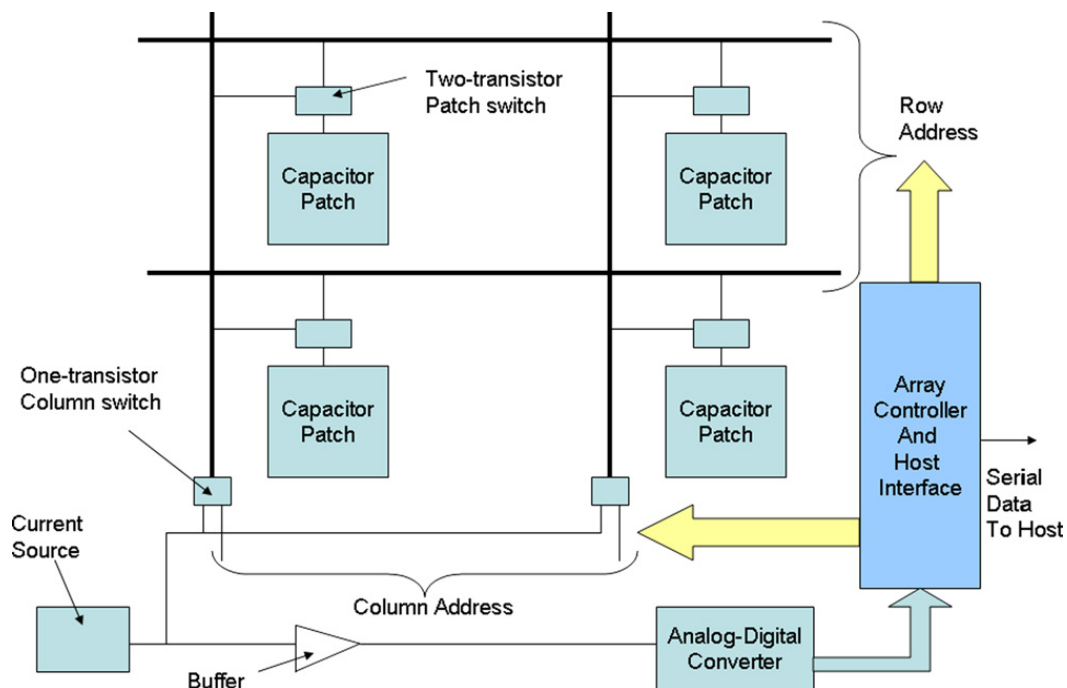


Fig. 10. Schematic of 2 × 2 capacitive sensor array readout electronics.

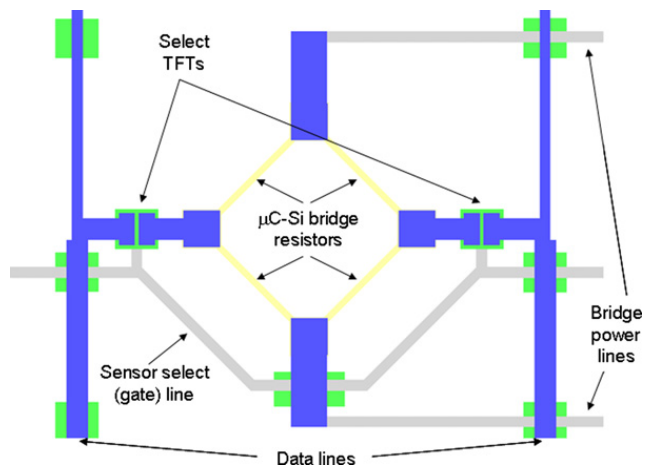


Fig. 11. Individual strain sensor layout schematic (shown with TFTs and bus connections).

A similar process used to fabricate the amorphous hydrogenated silicon ($a\text{-Si:H}$) TFTs (used for device selection and isolation in the sensor array) and the strain sensors on Kapton[®] polyimide substrates has been previously reported [31]. To facilitate handling the flexible substrate for the sensor fabrication processing, the Kapton[®] polyimide substrate is laminated to a glass carrier with a removable silicone gel adhesive layer to maintain substrate flatness and provide improved thermal control during processing. The TFTs employ $a\text{-Si:H}$ active material and a silicon nitride gate dielectric. The strain sensors are comprised of a n^+ microcrystalline silicon ($\mu\text{C-Si}$) thin film layer, which is deposited using the same method. The fabrication techniques used are compatible with polyimide materials, with the $a\text{-Si:H}$, $\mu\text{C-Si}$ and silicon nitride films deposited in a three-chamber plasma-enhanced chemical vapor deposition system at 250 °C. Devices and sensors are patterned using photolithography combined with hydrofluoric acid wet chemical etching, chlorine-based plasma etching or CFB_4 reactive ion etching [31]. After sample fabrication, the polyimide film is easily removed from the glass carrier for strain sensor testing. An actual device is shown in Fig. 12.

For testing, a current source is used to provide the input bias, and the output bridge signals are measured as voltages. Flexible cables are connected to the strain sensor using anisotropic conductive film bonding. A printed circuit board fan-out board provides interconnection of the flexible cable to multiple sensors fabricated on the same substrate. Three contacts are used to apply bias voltages (V_{B_d} , V_{B_s} and V_{B_g}), and two other contacts are used to measure output. Testing was accomplished using a combination of off-the-shelf data acquisition boards (from National Instruments) and custom circuit boards fabricated and assembled in house (Fig. 13). A National Instrument (NI) analog output board controlled the gate lines in addition to providing power to the sensors. An NI A/D converter read the outputs of the sensors and logged them into a personal computer (PC). NI software (LabView) was used to control the entire system from the PC.

Custom-made connectors were developed to interface with the purchased hardware. Additional signal condi-

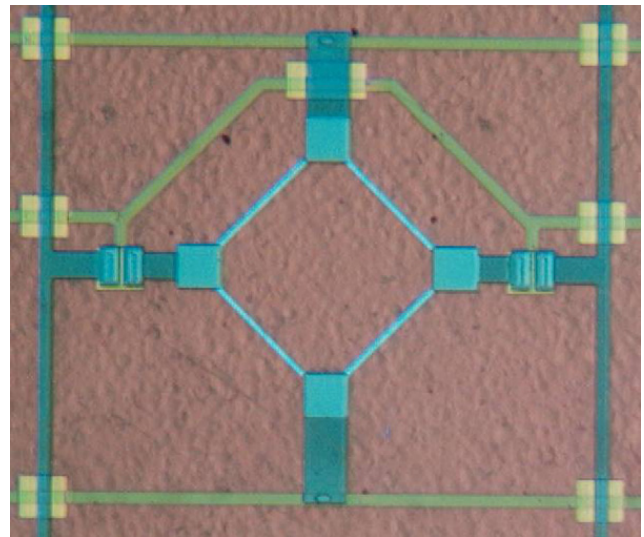


Fig. 12. Optical micrograph of fabricated sensor element on polyimide.

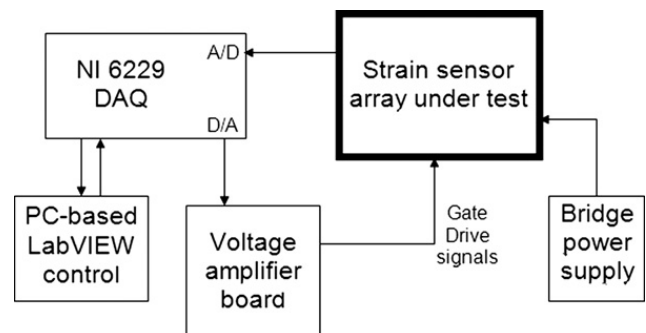


Fig. 13. Block diagram of test equipment.

tioning hardware was developed, to improve operation with the NI boards. A computer interrogation method was also developed, using a National Instruments 6229 data acquisition board and a Supertex HV257 high-voltage driver board, which supplies the required 25 V to the gate and across the source and drain. A single analog signal from the NI DAQ ranging from 0 to 5 V is used as input. Sensor outputs are connected to two fan-out boards, which are connected to the analog inputs of the NI data acquisition electronics. Fig. 14 shows the differential output of two of the sensors in a 2×2 array. The group of lines at 0 V is the output signals of other unbiased sensors in other small arrays. When the sensor is strained, a shift in the differential voltage amplitude is observed.

Straining the sample causes the voltages to shift (Fig. 14 right). The sample is strained in a concave diagonal direction, i.e., two corners of the sample are bent towards each other. A glass cylinder was used to provide a consistent bending radius for the orientation-dependent strain measurements (Fig. 15). The group of lines at 0 V is the output signals of other unbiased sensors in other small arrays on the same substrate. When the sensor is strained, the differential voltage lines of biased sensors shift as expected. Sensors in rows of the 2×2 arrays are in different orientations. The sensor perpendicular to the strain direction moves only ~ 20 mV. The sensor with bias current at an angle to the

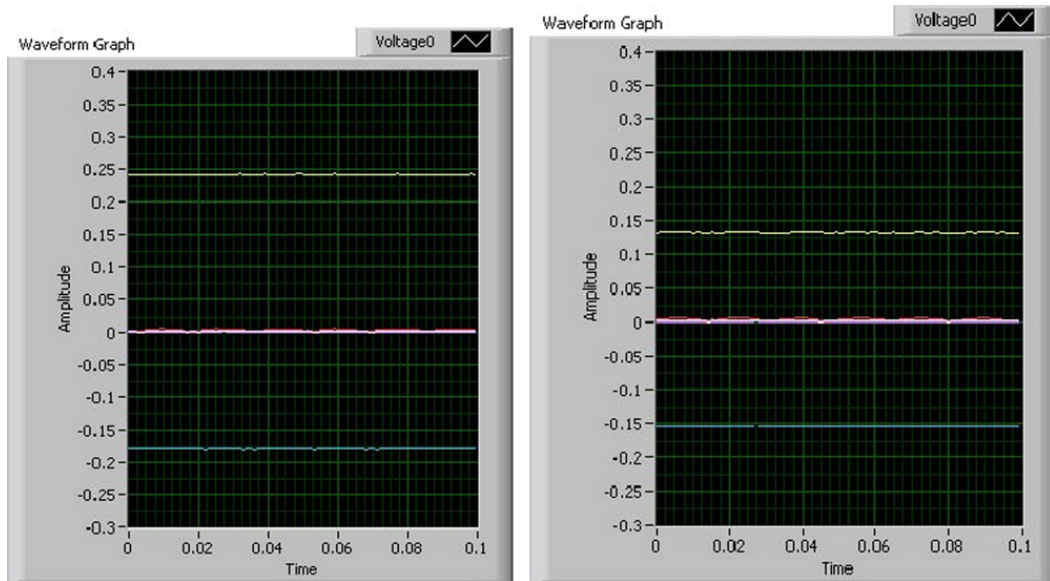


Fig. 14. Two sensors in the strain sensor array show a flat differential voltage amplitude (left). Straining the sample causes the voltages to shift (right).



Fig. 15. The sample is strained around a glass beaker to maintain a constant radius of curvature.

strain direction moves ~ 120 mV, illustrating the orientation dependence of the sensors as a differential output of two of the sensors in a 2×2 array. Ultimately, these data can be combined to develop a strain model for large area applications. This approach could be used to confirm habitat deployment, provide an alert if anomalous strain levels develop, provide information regarding dynamic loading, as well to monitor long term changes in the structure. Future efforts will focus on manufacturing arrays with larger numbers of unit cells on larger substrates, and integrating these switching electronics with the capacitive impact sensors (described in the previous sections) on the same substrate.

4.3. Passive wireless sensor tags

4.3.1. Theory of operation

In addition to damage detection and strain sensing, there is a need to integrate a range of other health

monitoring capabilities within inflatable/deployable structures. These include strike/impact detection accelerometers and ultrasonic/acoustic leak detectors for supplementing impact damage detection sensors. Other types of sensors may also provide important information about the state of the structure, including temperature sensors for characterizing thermal gradients, sensors for monitoring total radiation doses to the structure and even humidity/moisture sensors for monitoring buildup of moisture between habitat layers. In the case of blanket sensors of the type discussed in Section 4.1, access for power and data can be provided through the matrixed interconnects. In the case of widely distributed multiple point sensors where blanket coverage is not needed, however, achieving power distribution and data collection is challenging due to the complexity of integrating cabling and harnesses and implementing related feedthroughs and penetrations between the multi-layers (which must not interfere with the stowage and deployment processes).

One possible means to circumvent these limitations is to employ passive wireless sensor tags [39–43]. Unlike powered tags (that use their own DC electrical power, such as from batteries, power supplies, solar cells, etc.), passive tags rely solely on the radio-frequency (RF) energy transmitted from an interrogation device. Therefore, both *interrogation and power* for these passive devices is provided wirelessly, decoupling the sensors from the power bus and obviating the need for energy storage technologies, such as batteries. This offers a distinct advantage for integration of distributed sensors with an inflatable/deployable habitat.

To enable this type of passive remote sensing of physical properties requires transmission and sensing of an RF signal by means of an appropriate interrogation device. This device transmits an RF signal and receives a modified response from a sensor tag (analogous to radar). The response from the tag is modified in a manner proportional to the physical property being measured by the tag, such as temperature, acceleration, or light level.

To implement arrays of this type of sensor within inflatable/deployable habitats, it is essential to differentiate one particular tag of interest from other tags within range of the interrogator. For this effort, the tags were designed to respond to different narrow-frequency bands, with the interrogator selecting the tag of interest by changing the interrogation frequency. The narrow-frequency selectivity is accomplished at the tag by means of a surface acoustic wave (SAW) filter. SAW filters provide narrow frequency separation and conversion of variable impedance information into RF signal modulation. Sensors that vary impedance with respect to some physical parameter can thereby be measured remotely by measuring the proportional modulation in the RF return signal from the SAW filter.

The main elements of the passive remote sensing system, therefore, are a (1) small radio transmitter sending out a short burst of RF waves, (2) SAW-based tag both receiving and modifying a portion of that signal and (3) receiver to pick up the transmitted and modified pulse (Fig. 16). If the receiver and transmitter are in separate locations, the arrangement is bi-static.

At the heart of the sensor tag is the SAW filter (Fig. 17), which is a bandpass, frequency selective device that operates by converting electrical energy into acoustic energy in order to perform signal processing operations on the signal. The SAW filters discussed in this section are all three-port devices, meaning they possess three electrical-to-acoustic transducers, with one input and two output ports. The SAW filter is ultimately an acoustic device that delays the reflected signal from its output port, with the delayed signal containing the sensor measurement information.

An antenna is connected to the input port of the sensor tag SAW filter, and an impedance varying sensor is tied to the output port. The RF pulse is first received by the tag antenna and is converted into an acoustic wave by the input transducer of the SAW filter. The sensor tag varies its acoustically delayed radar cross section in proportion to the variable impedance load connected to the SAW output port. Variations in sensor impedance are caused by variations in the physical property to be measured. This, in turn, induces variations in the SAW filter's acoustic impedance. The variations in the filter's acoustic

impedance lead to variations in reflectance for a received RF wave. The reflectance of the acoustic wave is in proportion to the impedance of the sensor tied to that port. These variations are acoustically delayed and re-transmitted from the antenna at the input port of the SAW filter. The acoustic wave, therefore, travels across the SAW device and is reflected off of the output transducer of the SAW. The reflected acoustic wave travels back across the SAW, where it is ultimately re-transmitted by the antenna connected to the input port of the SAW.

The variations in the sensor impedance can then be detected as delayed amplitude variations in a received RF signal. In this manner, the sensor impedance can be measured back at the receiver. The SAW sensor must respond with sufficient efficiency to be detected by the receiver, since the RF return signal is weak. The proper application of a narrowband SAW filter, however, enables clear reception and measurement of the sensor impedance despite the relatively weak signal. Since it is acoustically delayed from the original RF excitation signal, the return signal can be read after all radar reflections induced within the vicinity of the transmitter have dissipated.

4.3.2. Testing of passive wireless sensor tags

To demonstrate the viability of implementing a passive wireless sensor tag concept within an inflatable/deployable habitat, a testbed for characterizing the response of various tags and sensors was established. The test arrangement for characterizing the sensor tag configuration is

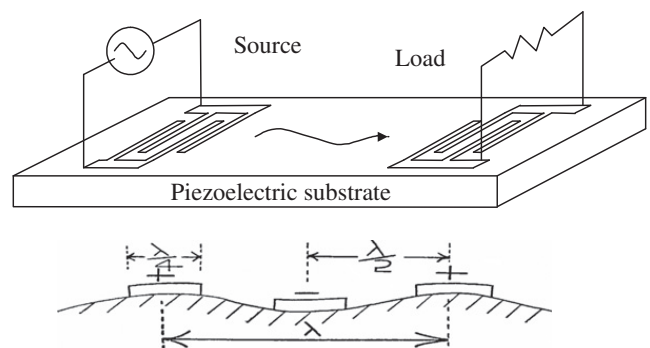


Fig. 17. Schematic representation of SAW devices.

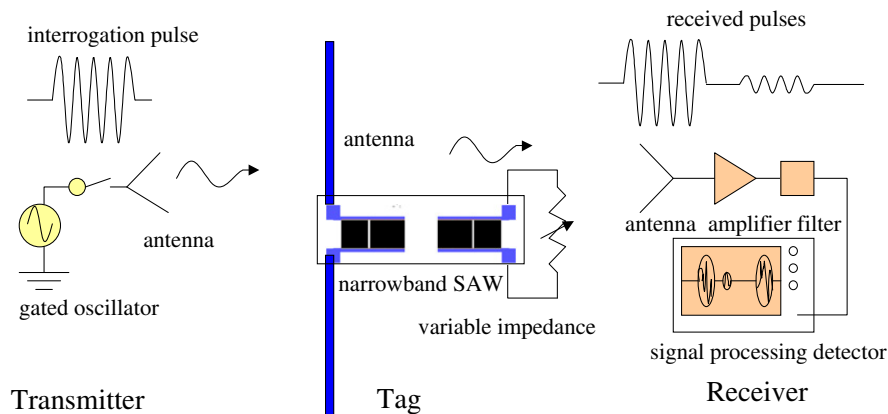


Fig. 16. Passive wireless sensor tag configuration.

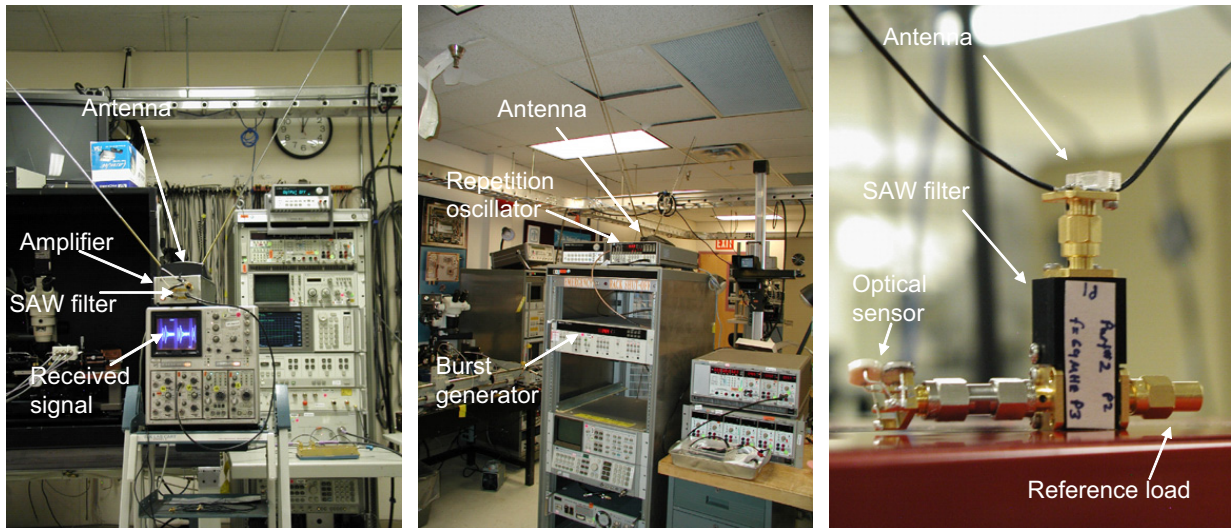


Fig. 18. Interrogator receiver (left), interrogator transmitter (center) and sensor tag (right).

shown in Fig. 18, depicting the three main elements of the test setup; the transmitter, the tag and the receiver. The receiver (Fig. 18 left) consists of an antenna tuned to the frequency band of interest, which, in turn, is connected to a SAW filter that is then connected through an amplifier to an oscilloscope. A more sophisticated receiver could include a gating device to block all return signals except for the acoustically delayed signal. This particular receiver did not include such a gating device. The transmitter (Fig. 18 center) consists of an RF burst generator pulsed repetitively by a low-frequency oscillator. The transmitter center frequency is at the exact center frequency of the SAW filter in the tag. The RF burst generator is connected directly to an antenna without an additional amplifier. The tag (Fig. 18 right) consists of an antenna coupled directly to a narrowband SAW filter. The SAW filter (Fig. 19) actually consists of two SAW filters operating in parallel. Both SAW filters have their input ports tied directly to the antenna, and their output ports tied to resistive loads. The first SAW filter serves as a reference arm of the sensor. It is attached to a fixed 50-Ω resistance. The second SAW filter is tied to the impedance-changing sensor. The sensor can be an accelerometer, a light sensor, a thermistor, or any other impedance-varying device.

The testbed shown in Fig. 18 is sufficiently general to enable the testing of a wide variety of different sensors. Any sensor that varies its impedance in some relation to the physical quantity to be measured can be used as a wireless SAW sensor. The entire SAW sensor configuration is not actively powered, and can therefore be permanently configured without batteries or a power source, which is ideal for inflatable/deployable structures.

A total of five different classes of sensors were characterized using the wireless SAW sensor testbed, including a mechanical switch, a temperature transducer, accelerometer and two light sensors (a photoconductor and a phototransistor). The raw signals received from a switch in the closed and open positions are shown in Fig. 20 top left and top right, respectively. The magnitude of the reference signal is not dependent on the position of

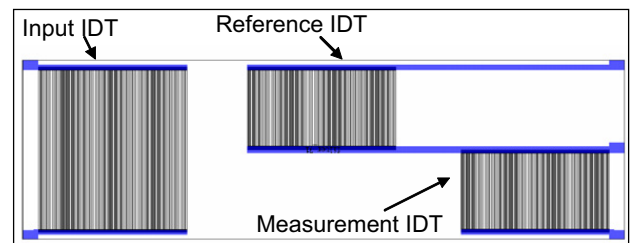


Fig. 19. SAW filter used for wireless remote sensing. Note the layout of the interdigitated transducers (IDT).

the switch. The delayed, re-transmitted measurement signal varies strongly with switch position, as can be seen by comparing the two photos. Many extraneous factors can cause both the reference and the measurement signals to vary in tandem, but only the switch position causes the relative difference in the two signals to change.

The results of measuring the accelerometer remotely are also shown in Fig. 20. The accelerometer used was an Endevco 2221F piezoelectric device. Fig. 20 (middle left) shows the accelerometer with no excitation. The delayed response has a peak magnitude of about 80 mV, corresponding to an open circuit condition. Fig. 20 (middle right) shows the accelerometer response as the accelerometer is receiving a shock. The configuration provides signal integration, so that the charge from the shock acceleration is stored and made available for approximately 1 s. This time constant can be varied from a maximum of about 1 s to as fast as the time constant of the shock or the accelerometer, whichever is slower.

Finally, the results of remotely measuring a photodetector are shown in Fig. 20. The photodetector used here was a cadmium sulfide (CdS) device with an impedance that varies between 400 Ω under dim light and 35 Ω when placed directly under a 60-W incandescent bulb. The results are similar to those described for the previous sensors. Under dim light, the tag delayed response was approximately 40 mV peak-to-peak. Under bright light, the tag delayed response increased to

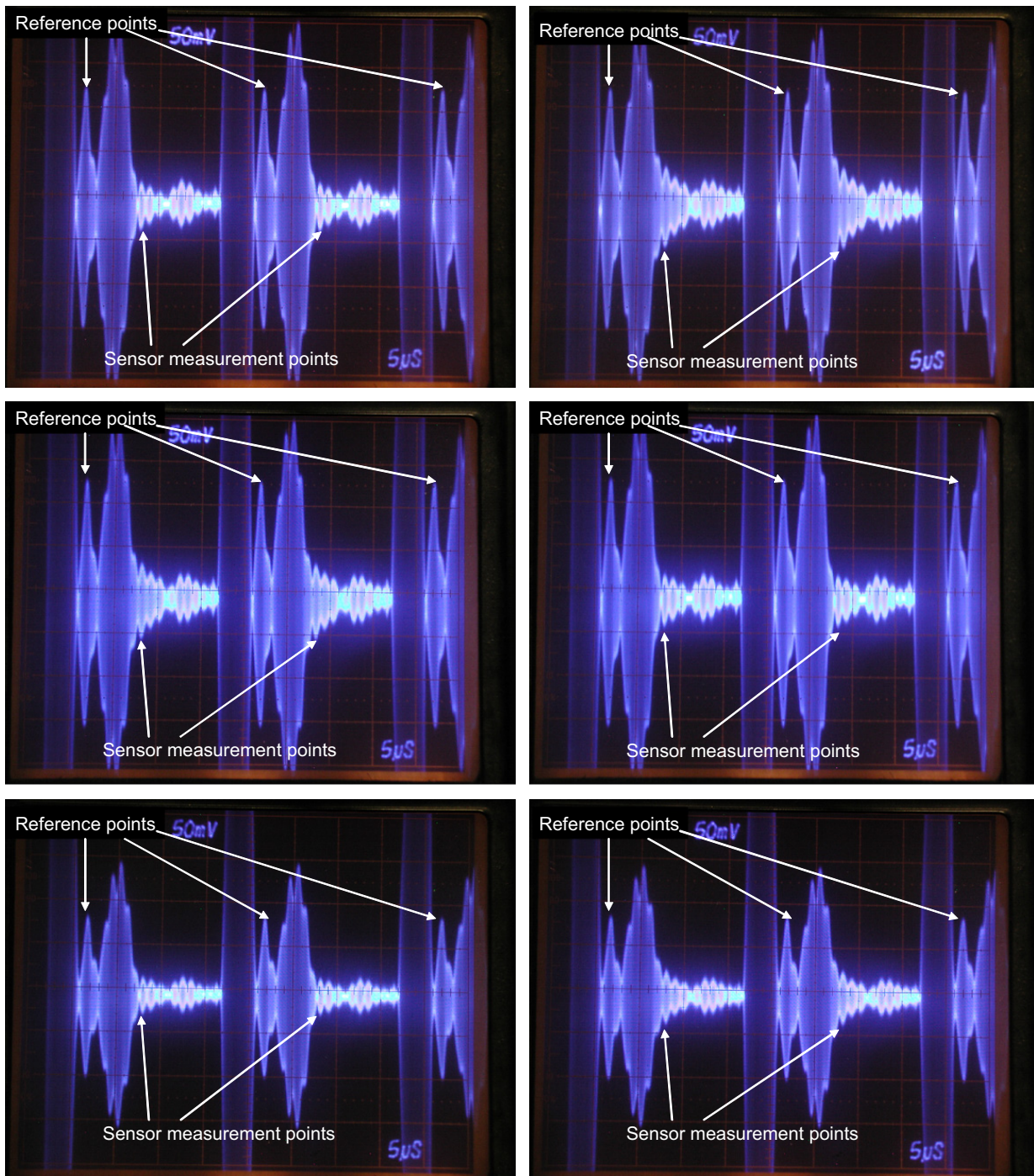


Fig. 20. Sensor tag measurements from three different sensors, switch response in closed position (*top left*) and open position (*top right*); accelerometer with no excitation (*middle left*) and receiving a shock (*middle right*); photodetector in dim light (*bottom left*) and bright light (*bottom right*).

approximately 60 mV. An increased signal response can be obtained using a photodetector with lower impedance.

This ability to detect impedance variations and their consequent variations in delayed responses in the received signals using three different sensor types clearly demonstrates the flexibility of this approach, and opens the door to integrate a wide variety of sensors within habitats which require no hardwired power or data acquisition connection. The key is to identify appropriate sensors for integration with the SAW based tag. The use of these multiple sensor types indicates the potential for

widespread use in habitats. Further efforts will build on these initial results, focusing on issues of signal attenuation when incorporated into representative habitat materials.

5. Self-healing flexible laminates for bladders

5.1. Background

The ultimate goal in inflatable/deployable habitat design is to develop semi-autonomous structures which

have the capability to adapt to changing circumstances. One step in this evolution toward autonomy is the incorporation of a “self-healing” functionality. It is envisioned that integrated sensing technologies could be used effectively in conjunction with self-healing materials, indicating when damage occurs, monitoring the self-healing process as it proceeds and ultimately notifying the crew if the damage is such that human intervention is required.

The consideration of such a capability for inflatable/deployable habitats and structures is enabled by recent development in self-healing polymers. Self-healing polymers are inspired by living systems, in which minor damage (e.g., a bump or bruise) triggers an autonomic healing response [44]. In biological systems, chemical signals released at the site of fracture initiate a systemic response that transports healing agents to the site of injury and promotes healing. Recent research efforts at the University of Illinois [44,47–51] have led to the successful engineering of a self-healing epoxy that mimics many of the features of a biological system. Fig. 21 illustrates this concept, wherein healing is accomplished by incorporating a microencapsulated healing agent and a polymerization initiator within a polymer matrix. Damage in the form of a crack or tear serves as the triggering mechanism for self-healing, similar to the fracture event in biological systems. The approaching crack ruptures the embedded microcapsules, releasing healing agent into the crack plane through capillary action. Polymerization of the healing agent is triggered by contact with the initiator, bonding the crack faces. As with biological systems, this triggering mechanism provides site-specific control of healing.

The self-healing concept depicted in Fig. 21 is not practical for mitigating large-scale micrometeoroid damage of habitats, but it may be able to provide efficient repair of smaller scale bladder damage, or even internal matrix cracking or delamination in rigidizable structural elements. A self-healing bladder material is one of the most appealing candidates, as this layer must contain the breathable volume of air in which the crew will live and work. In addition to safety issues, recent experience in the ISS has demonstrated that detecting small leaks in large structures is a time consuming process. The ability for the bladder to “self-seal” small leaks could minimize crew time spent locating and repairing leaks.

Bladder materials [6] for an inflatable space habitat must meet several requirements, including sufficient flexibility in a space environment, low oxygen permeability, puncture and tear resistance and minimal off-gassing. Laminate materials are most frequently considered for space-based bladder applications. Polyurethane laminations with Kevlar, polyester [45], Saran and Tedlar are materials currently being considered for use as habitat structural materials. Silicone-coated Vectran has been proposed as a bladder material due to its suitable properties at low temperatures behavior and material simplicity. Laminates with commercial food packing films such as ethylene vinyl alcohol and Combitherm [46] have also been proposed as bladder materials. Two other commercial materials that are currently used as bladders

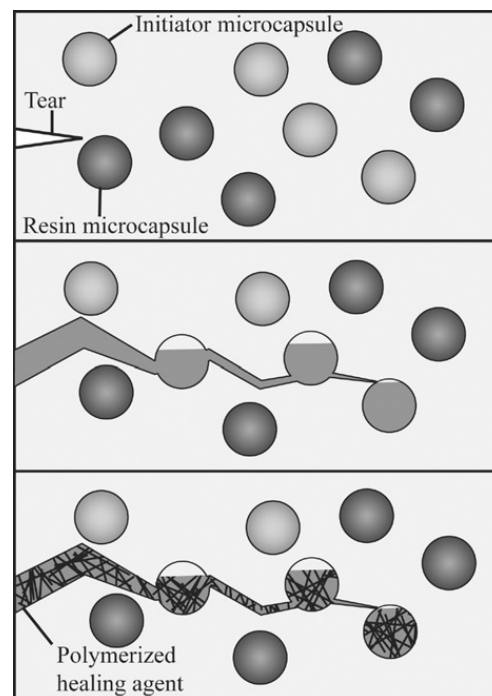


Fig. 21. Microencapsulated self-healing elastomer concept.

for space-borne structures include Cepac HD200 [5], a nylon/PE/Valeron/PE/foil/coex laminate and ArmorFlex, a thermoplastic urethane laminated to a nylon basecloth. These laminated bladder materials range from 5 to 15 mil (25.4 $\mu\text{m}/\text{mil}$) in thickness. The TransHab design specifies a redundant bladder system in which three individual bladders are separated by Kevlar felts (bleeder cloths) to provide additional puncture resistance. A single-bladder design makes stowage and deployment easier, but is riskier due to the lack of redundancy.

The bladder materials listed above all share one defining characteristic in that they are flexible. Most recent work to date in the area of self-healing materials, however, has been in the context of thermosetting polymers such as epoxies which are generally not highly pliable. Thus, the development of new approaches and new materials are required to include self-healing functionality in a flexible, foldable bladder structure. To address the need for a flexible self-healing material, a new self-healing elastomer was developed as part of this SHMS development project. The elastomer is capable of regaining significant amounts of its virgin tear strength [47]. This microcapsule-based material is also tougher than the neat, unfilled material based on tear energies derived from trouser-tear results.

5.2. Self-healing poly(dimethylsiloxane) system

A self-healing elastomer consists of a poly(dimethylsiloxane) (PDMS) elastomer matrix with embedded microcapsules. These microcapsules contain, in separate capsules, a vinyl-terminated poly(dimethylsiloxane) resin and a methylhydrosiloxane copolymer. These two materials react via a platinum catalyzed hydrosilylation reaction, outlined in Fig. 22. The Pt catalyst complexes are in

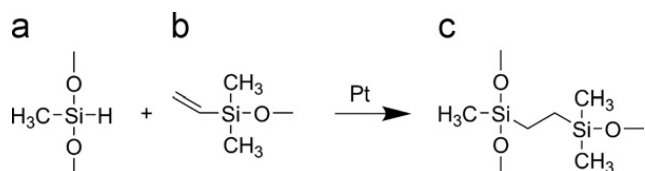


Fig. 22. Hydrosilylation reaction of (a) vinyl-terminated poly(dimethylsiloxane) to a (b) methylhydrosiloxane copolymer backbone forming (c), a crosslinked polysiloxane elastomer via the action of a platinum catalyst.

solution with the vinyl-terminated resin and encapsulated in the same capsule as the resin material.

PDMS was chosen as the first test material because of its high strain to failure (~200%), room temperature cure, and the wide variety of adhesion promoting coupling agents. A commercial two-part PDMS system, Sylgard 184 (Dow Corning, USA), functioned as the matrix and provided the resin and initiator materials for the healing chemistry. Resin and initiator were encapsulated in a urea-formaldehyde polymer shell using the procedure outlined previously by Brown et al. [53]. The initiator was encapsulated as received, but the resin was thinned by the addition of 20-wt% heptane solvent.

The two microcapsules were incorporated into the premixed matrix material by mechanical mixing. A pre-curing period of at least 4 h was employed before capsule introduction, to minimize floating of the buoyant initiator capsules. The self-healing material was then poured into an open metal mold and allowed to cure for 48 h at room temperature. Samples were then removed from the mold and prepared for testing.

5.3. Healing efficiency for elastomers

As part of the current effort, a new test protocol was developed to quantify healing performance for these elastomeric materials based on the recovery of tear strength. Self-healing elastomer samples were tested using the trouser-tear test developed and analyzed by Greensmith and Thomas [54]. Samples were rectangular and nominally between 1.5 and 2 mm thick. A representative tear sample is shown in Fig. 23 (a). The center cut forming the legs of the tear specimen was introduced by hand with a razor blade. Samples were tested within a few minutes after the initial center cut was made. The samples were gripped at the end of each of the legs formed by the center cut and loaded in tension to failure with a crosshead speed of 250 mm/min. The tear strength, T^{avg} , was calculated by averaging the tear force within the tearing region of the load–displacement plot and then using the relationship:

$$T^{avg} = \frac{2F^{avg}}{t}, \quad (3)$$

where F^{avg} is the averaged tearing force and t is the sample thickness, to determine the tear strength of the specimen.

After the initial tear, the samples were stored between two glass microscope slides to ensure that the tear surfaces came back into contact with each other. After

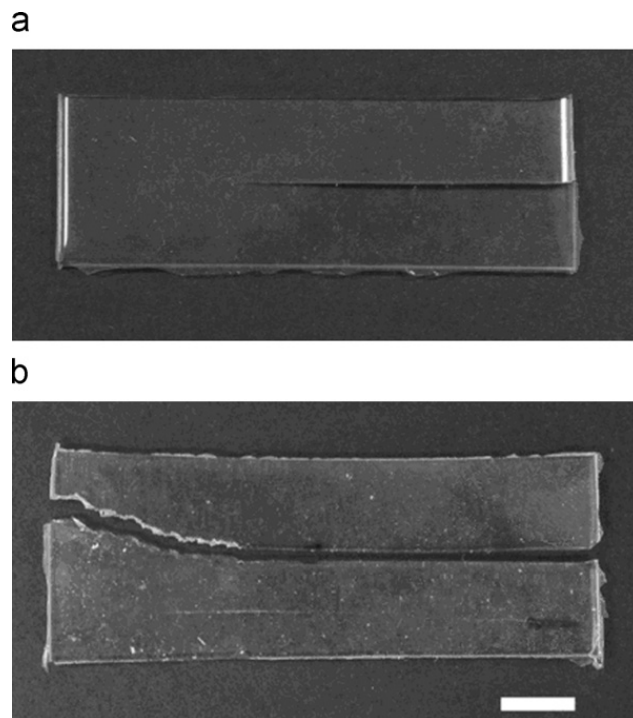


Fig. 23. (a) Tear specimen prior to virgin testing and (b) failed tear specimen.

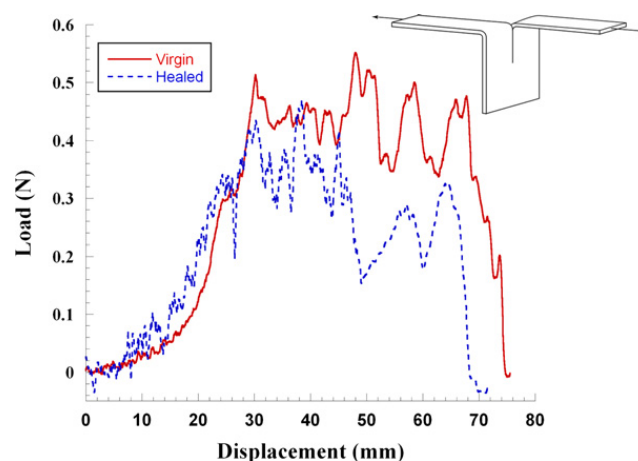


Fig. 24. Representative load–displacement traces for a virgin and healed tear test.

healing, the samples were removed from the slides, the tear was reopened to the original starting point, and the samples were tested again. Healing efficiency η is defined in the equation below as the recovery of tear strength T ,

$$\eta = \frac{T^{avg}_{healed}}{T^{avg}_{virgin}}. \quad (4)$$

5.4. Self-healing results

Representative load–displacement plots for a virgin and healed tear test of a fully *in-situ* specimen are shown in Fig. 24. All PDMS tear specimens exhibited stick–slip tearing behavior regardless of capsule concentration, as expected for filled elastomers [55].

To assess the effectiveness of the healing mechanism, the fully *in-situ* system was compared to a series of control tests. Fig. 25 is a comparison of the healing performance of the three control specimens and the fully *in-situ* material system. All of the values reported in Fig. 25 are averages of at least six specimens. The neat specimens were PDMS tear specimens containing no healing components. These specimens were tested to determine the contribution of surface cohesion to any healing response. Neat specimens recovered just a few percent of their original tear strength and generally fell apart while preparing each specimen for testing. The second control contained only resin-filled microcapsules. These specimens failed to effectively heal, attaining healing efficiencies of only a few percent. Specimens containing 5 wt% initiator copolymer containing microcapsules, however, exhibited a significant recovery of original tear strength, approaching healing efficiencies of 40%. The healing in these specimens is attributed to the interaction of the initiating copolymer with excess vinyl functionality in the surrounding matrix. Further polymerization leads to a modest recovery of original tear strength. Fully *in-situ* specimens contained 5 wt% resin and 5 wt% initiator microcapsules.

These specimens recovered nearly 95% of the virgin tear strength and in some cases exceeded the virgin tear strength. Healing efficiencies greater than 100% were achieved when the tear deviated from the original tear line into virgin material. This failure could occur in one of two ways: a complete deviation, in which the tear proceeded in a new line through the remainder of the sample, or a partial deviation, such that the tear deviated into new material but then returned to the original line. A tear line characterized by the second case could leave and return to the healed tear line multiple times. The scanning electron microscope image in Fig. 26 shows a tear deviation highlighted on the top surface of the tear specimen, viewed parallel with the tear plane. The 1st virgin test is labeled and highlights the adhesive bond line

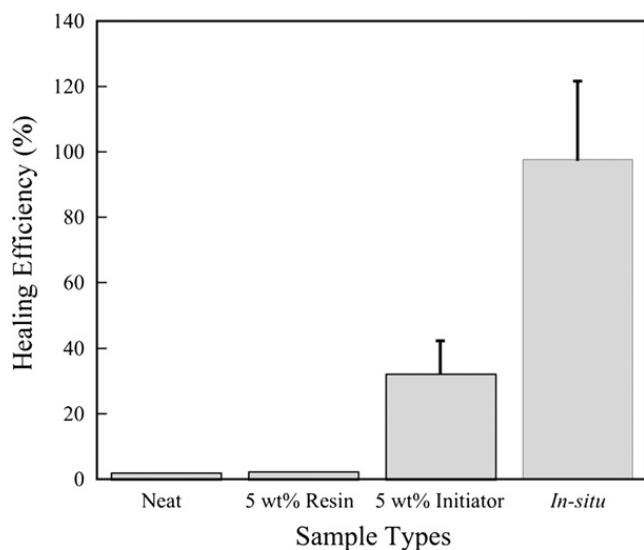


Fig. 25. Healing efficiencies of controls and the fully *in-situ* (5 wt% resin and initiator) specimens.

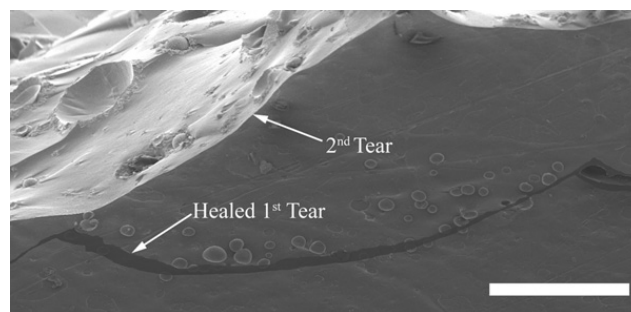


Fig. 26. Scanning electron microscope image of healed tear specimen viewed parallel to the tear plane (2nd tear labeled in image). The healed 1st tear is highlighted. The scale bar is equivalent to 200 μm .

generated from released capsule contents. The 2nd tear propagated independent of the virgin line, following a new path through the specimen. Even though the new tear passes close to healed tear, the tear does not turn into and run along the bond line.

5.5. Approaches to developing a self-healing bladder material

Bladder damage due to failure of the MMOD shield or caused by a puncture from the inside of the habitat is highly undesirable. Damage induced by handling and deployment or from daily activity within the habitat is also a concern and a candidate for self-healing. One significant challenge for creating a successful self-healing bladder is the incorporation of microcapsules containing healing agent and catalyst into a thin, laminated elastomeric film. Continued development of healing chemistries that can seal tears, cracks and punctures in a thin, flexible polymer and careful evaluation of the potential failure modes in these materials is required to identify limitations on the types of damage that can be healed. Any self-healing material must also meet specific operational demands in order to optimally function as a bladder material: it must remain flexible in a space environment, have low oxygen permeability, resist puncture and tearing damage and have minimal offgassing.

There are two options for incorporating self-healing functionality into bladder materials. One option is to manufacture a bladder material that contains a directly incorporated self-healing system. The second option is to apply a self-healing layer to an existing bladder material. The first option is a fully integrated self-healing bladder material that contains, as part of the material structure, an integrated self-healing functionality. Conceptually, the bladder material becomes a film version of the original self-healing system developed by White et al. [44], where capsules or some other mechanism are incorporated into the material at the manufacturing level. Since most of the candidate systems are laminated film structures, the self-healing functionality could be incorporated throughout the entire laminated structure, or just in a few layers. Although this provides the most integrated approach, it also introduces a number of manufacturing challenges. Microcapsules must be reduced in diameter to physically fit into the thin layers that make up many bladder

materials. Any self-healing components must also be robust enough to survive the manufacturing process, which may include high temperatures and pressures. These are significant challenges, but recent progress in both reducing healing component dimensions [56] and improving high temperature stability has been made [57]. The second option is to apply a self-healing coating on one side of the bladder. This approach avoids many of the manufacturing issues associated with the integrated approach described above. Application of a separate film layer, however, requires careful selection of bladder and coating materials to ensure good adhesion.

5.6. Prototype self-healing bladder membrane

Using the applied-healing-layer approach for the construction of a self-healing bladder, a prototype material has been developed using the self-healing PDMS sandwiched between two barrier layers. This material, shown in Fig. 27, has demonstrated the capability of sealing small puncture and cut damage under static conditions.

A static pressure test was conducted, wherein the material was damaged either by a puncture or a small cut. Following a healing period of 24 h, the healed membrane was then subjected to a pressure test using a custom built test cell. Healing was characterized by one of three behaviors. If the membrane held 15 psi without leakage, the membrane was considered “fully healed.” If the membrane held pressure without leakage, but ruptured and began leaking before 15 psi was reached, it was considered “partially healed.” If a membrane leaked immediately upon application of any pressure it was considered “not healed.” Healing response of the self-healing membranes for a variety of puncture diameters is shown in Fig. 28 (each bar represents the healing probability for six samples).

For small puncture damage (~ 0.5 mm) healing exceeds 50%. Small punctures are the primary mode of damage that a self-healing/sealing bladder material is envisioned to address. As such, even the first stage prototype, shown in Fig. 27, has achieved considerable success. Further possible refinements to the prototype material include an optimization of capsule size and distribution, an analysis of the effect of healing layer thickness on healing performance and an investigation of healing chemistry and kinetics.

It is important to note that self-healing to date has only been demonstrated under ambient, terrestrial conditions. The space environment introduces numerous unique environmental conditions, including reduced pressure, low temperature and radiation. Determining how the

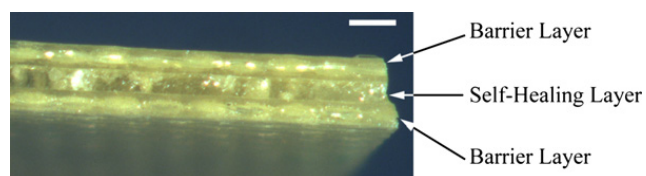


Fig. 27. Edge of prototype self-healing bladder. Scale bar is equal to 500 μm .

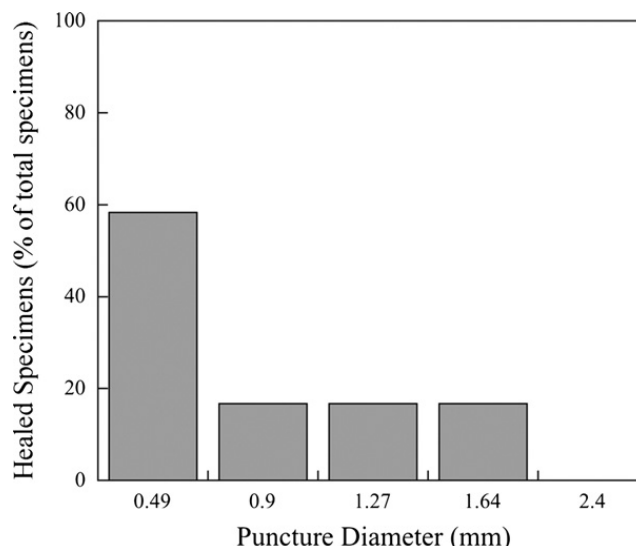


Fig. 28. Healing performance of prototype flexible laminate.

space environment influences the mechanics and chemistry of self-healing is of paramount importance. The main hazards of the space environment for polymers include high vacuum, ionizing radiation and extreme temperatures [52]. In low earth orbit, additional factors are operative including solar UV radiation and atomic oxygen [52]. Key issues for the successful accomplishment of self-healing in space structures are to assess, understand and solve environmental stability issues associated with: (1) outgassing from high vacuum conditions, (2) radiation effects on self-healing polymers and (3) maintaining self-healing functionality at cryogenic temperatures.

6. Conclusion

Inflatable/deployable structures are currently under development for commercial space efforts, and will likely play a role in future NASA human exploration efforts to the Moon and beyond. To ensure the safety of humans in future NASA missions involving these types of structures, efforts have focused on the integration of sensor technologies capable of monitoring the health of the structure. Toward this end, technologies meeting the unique requirements of inflatable habitats are currently under development, including both flexible and passive wireless sensors. As a next step in the evolution of habitat capabilities, self-healing materials are also being developed, to increase the autonomy of these structures. The development and testing of prototype sensing and self-healing technologies specifically designed for these structures have been reported herein. The ultimate goal is to combine both sensing and self-healing capabilities within the same structure, to work synergistically to provide a safer human space habitat.

Acknowledgements

The authors thank Chris Moore of NASA Headquarters and Judith Watson of NASA Langley Research Center for

their guidance and support during this project, Benny Toomarian, Mohammad Mojarradi and Anil Thakoor of JPL for helpful discussions and John Frassanito and Associates for the use of the habitat images. This work was performed by the Jet Propulsion Laboratory, California Institute of Technology through the support of the NASA Exploration and Science Mission Directorate.

References

- [1] P.D. Spudis, The moon and the new presidential space vision, *Earth Moon Planets* 94 (2005) 213–219.
- [2] K.J. Kennedy, M.P. Cerimele, *Habitation and Human Systems for the 90 Day Study*, NASA Publication JSC-24398, Houston, TX, 1990.
- [3] G.B. Ganapathi, J. Ferrall, P.K. Seshan, *Lunar Base Habitat Designs: Characterizing the Environment and Selecting Habitat Designs for Future Trade-offs*, JPL Publication 93-20, Pasadena, CA, 1993.
- [4] K.H. Merkel, J.M. Alexander, *Expandable lunar shelter concepts*, Aerospace Expandable Structures Conference Transactions, Air Force Aero Propulsion Laboratory, Dayton, OH, 1963.
- [5] R.T. Bigelow, Bigelow Aerospace, US patent for inflatable satellite bus, US Patent 6962310, 2005.
- [6] D. Cadogan, J. J. Stein, M. Grahne, *Inflatable composite habitat structures for Lunar and Mars exploration*, *Acta Astronaut.* 44 (1999) 399–406.
- [7] K.J. Kennedy, J. Raboin, G. Spexarth, G. Valle, *Inflatable habitats*, in: C.H.M. Jenkins (Ed.), *Gossamer Spacecraft: Membrane and Inflatable Structures Technology for Space Applications*, AIAA, 2000, pp. 527–552.
- [8] K.J. Kennedy, *Lessons from TransHab, an architect's experience*, in: AIAA Space Architecture Symposium Proceedings, AIAA, 2002, pp. 1–11.
- [9] H. de la Fuente, J. Raboin, G.R. Spexarth, G.D. Valle, *TransHab: NASA's large-scale inflatable spacecraft*, in: *Proceedings of the 2000 AIAA Space Inflatables Forum; Structures, Structural Dynamics, and Materials Conference*, AIAA, 2000, pp. 1–9.
- [10] K.J. Kennedy, S.D. Capps, *Designing space habitation*, in: *Proceedings of Space 2000: The Seventh International Conference and Exposition on Engineering, Construction, Operations, and Business in Space*, ASCE, 2000, pp. 49–71.
- [11] K.J. Kennedy, *A horizontal inflatable habitat for SEI*, in: *Proceedings of the 3rd International Conference on Engineering, Construction, and Operations in Space III*, AIAA, 1992, pp. 135–146.
- [12] K.J. Kennedy, *Inflatable habitat option for a human lunar return mission*, in: *SPACE V, Proceedings of the Fifth International Conference on Space*, ASCE, 1996, pp. 1077–1082.
- [13] G.D. Badhwar, H. Huff, R. Wilkins, S. Thibeault, *Comparison of graphite, aluminum, and TransHab shielding material characteristics in a high-energy neutron field*, *Radiat. Meas.* 35 (2002) 545–549.
- [14] P.S. Nowak, W.Z. Sadeh, J. Janakus, *Feasibility study of inflatable structures for a lunar base*, *J. Spacecr. Rockets* 31 (1994) 453–457.
- [15] J. Day, P. Richter, *Analyses of lunar membrane structures for potential failure scenarios*, in: *SPACE V, Proceedings of the Fifth International Conference on Space*, ASCE, 1996, pp. 1052–1058.
- [16] M.E. Criswell, W.Z. Sadeh, J. Abarbanel, *Design and performance criteria for inflatable structures in space*, in: *SPACE V, Proceedings of the Fifth International Conference on Space*, ASCE, 1996, pp. 1045–1051.
- [17] D.M. Langlais, D.P. Saulnier, *Reusable, pressurized dome for lunar construction*, in: *Proceedings of Space 2000: The Seventh International Conference and Exposition on Engineering, Construction, Operations, and Business in Space*, ASCE, 2000, pp. 791–797.
- [18] P.S. Nowak, M.E. Criswell, W.Z. Sadeh, *Inflatable structures for a lunar base*, in: *Proceedings of Space 90, Engineering, Construction and Operations in Space*, ASCE, 1990, pp. 510–519.
- [19] P.K. Yin, *Structural design of an inflatable habitat*, in: *Proceedings of Space 90, Engineering, Construction and Operations in Space*, ASCE, 1990, pp. 520–528.
- [20] T.A. Bateman, J.E. Abarbanel, M.E. Criswell, *Structural modifications to the framing system of a proposed Lunar/Martian habitat*, in: *Proceedings of Space 2000: The Seventh International Conference and Exposition on Engineering, Construction, Operations, and Business in Space*, ASCE, 2000, pp. 424–430.
- [21] R.M. Suggs, W.J. Cooke, R.J. Suggs, W.R. Swift, N. Hollon, *The NASA lunar impact monitoring program*, *Earth Moon Planets* 102 (2008) 293–298.
- [22] J.M. Sater, C.R. Crowe, R. Antcliff, A. Das, in: A.K. Noor (Ed.), *Structures and Technology for Future Aerospace Systems*, Aerospace Press, 2000, pp. 269–349.
- [23] S. Tung, S.R. Witherspoon, L.A. Roe, A. Silano, D.P. Maynard, N. Ferraro, *A MEMS-based flexible sensor and actuator system for space inflatable structures*, *Smart Mater. Struct.* 10 (2001) 1230–1239.
- [24] R.H. Reuss, B.R. Chalamala, A. Moussessian, M.G. Kane, A. Kumar, D.C. Zhang, J.A. Rogers, M. Hatalis, D. Temple, G. Moddel, B.J. Eliasson, M.J. Estes, J. Kunze, J.E.S. Handy, E.S. Harmon, D.B. Salzman, J.M. Woodall, M.A. Alam, J.Y. Murthy, S.C. Jacobsen, M. Olivier, D. Markus, P.M. Campbell, E. Snow, *Macroelectronics: perspectives on technology and application*, *Proc. IEEE* 93 (2005) 1239–1256.
- [25] M. Chason, D.R. Gamota, P.W. Brazis, K. Kalyanasundaram, J. Zhang, K.K. Lian, R. Crosswell, *Toward manufacturing low-cost, large-area electronics*, *MRS Bull.* 31 (2006) 471–475.
- [26] Y.L. Loo, I. McCulloch, *Progress and challenges in commercialization of organic electronics*, *MRS Bull.* 33 (2008) 653–662.
- [27] V.J. Lumelsky, M.S. Shur, S. Wagner, *Sensitive skin*, *IEEE Sens. J.* 1 (2001) 41–51.
- [28] L. Minbang, K. Heping, *A thin-film strain gauge tactile sensor array for robots*, in: *Proceedings of the Fifth International Conference on Advanced Robotics*, IEEE, 1991, pp. 1734–1737.
- [29] G. de Cesare, M. Gavesi, F. Palma, B. Ricco, *A novel a-Si:H mechanical stress sensor*, *Thin Solid Films* 427 (2003) 191–195.
- [30] T. Someya, Y. Kato, T. Sekitani, S. Iba, T. Noguchi, Y. Murase, H. Kawaguchi, T. Sakurai, *Conformable, flexible, large-area networks of pressure and thermal sensors with organic transistor active matrices*, *Proc. Natl. Acad. Sci.* 102 (2005) 12321–12325.
- [31] L. Zhou, S. Jung, E. Brandon, T.N. Jackson, *Flexible substrate microcrystalline silicon and gated amorphous silicon strain sensors*, *IEEE Trans. Electron Dev.* 53 (2006) 380–385.
- [32] E. Brandon, W. West, L. Zhou, T. Jackson, G. Theriot, R.A.B. Devine, D. Binkley, N. Verma and R. Crawford, *Flexible electronics for space applications*, in: *Flexible Electronics Symposium Proceedings*, MRS, San Francisco, CA, 2004, pp. 219–230.
- [33] E.J. Brandon, E.E. Wesseling, V. Chang, W.B. Kuhn, *Printed microinductors on flexible substrates for power applications*, *IEEE Trans. Compon. Packag. Technol.* 26 (2003) 517–523.
- [34] E.J. Brandon, W. West, E. Wesseling, *Carbon-printed contacts for organic thin-film transistors*, *Appl. Phys. Lett.* 83 (2003) 3945–3947.
- [35] R.J. Naumann, *Pegasus satellite measurements of meteoroid penetration*, *NASA Technical Memorandum X-1192*, 1965.
- [36] J.A.M. McDonnell, *The Giotto dust impact detection system*, *J. Phys. E: Sci. Instrum.* (1987) 741–758.
- [37] N.D. Semkin, L.S. Novikov, K.E. Voronov, D.G. Bobbin, R.A. Pomelnikov, S.V. Rotov, *Detector of micrometeoroid and artificial space debris particles*, *Space Debris* 2 (2000) 273–293.
- [38] S.E. Woodard, B.D. Taylor, T.W. Jones, Q.A. Shams, F. Lyons, D.A. Henderson, *A method to have multi-layer thermal insulation provide damage detection*, in: *Proceedings of the 48th AIAA/ASME/ASCE/AHS/ASC Structures, Structural Dynamics, and Materials Conference*, AIAA 2007-1847, Honolulu, HI, 2007, pp. 1–23.
- [39] K. Finkenzeller, *RFID Handbook*, 2nd ed., John Wiley and Sons, London, 2003, pp. 11–28.
- [40] C.K. Campbell, *Surface Acoustic Wave Devices for Mobile and Wireless Communication*, Academic Press, San Diego, 1998, p. 11.
- [41] K. Tsubouchi, N. Mikoshiba, *Zero-temperature-coefficient SAW devices on AlN epitaxial films*, *IEEE Trans. Sonics Ultrason.* SU-32 (1985) 634–644.
- [42] C. Hausleitner, R. Steindl, A. Pohl, H. Hauser, A.M.J. Goiser, F. Siefert, *Cordless batteryless wheel mouse application utilizing radio requestable SAW devices in combination with the giant magneto-impedance effect*, *IEEE Trans. Microwave Theory Techn.* 49 (2001) 817–822.
- [43] A. Pohl, *A review of wireless SAW sensors*, *IEEE Trans. Ultrason. Ferroelectr. Freq. Control* 47 (2000) 317–332.
- [44] S.R. White, N.R. Sottos, P.H. Geubelle, J.S. Moore, M.R. Kessler, S.R. Sriram, E.N. Brown, S. Viswanathan, *Autonomic healing of polymer composites*, *Nature* 409 (2001) 794–797.
- [45] K. Komatsu, M. Sano, Y. Kakuta, *Development of high specific-strength envelope materials*, in: *Proceedings of the AIAA Third Annual Aviation Technology, Integration and Operations Technology Forum*, AIAA, 2003.
- [46] G.A. Sanchez, E.L. Christiansen, J.H. Kerr, *Development of the ISS TransHab Module Meteorite and Orbital Debris Shield (Phase I to IV)*, NASA Publication JSC-28173, Houston, TX, 1997.

- [47] M.W. Keller, S.R. White, N.R. Sottos, A self-healing poly(dimethyl siloxane) elastomer, *Adv. Funct. Mater.* 17 (2007) 2399–2404.
- [48] M.R. Kessler, N.R. Sottos, S.R. White, Self-healing structural composite material, *Composites Pt. A: Appl. Sci. Manuf.* 34 (2003) 743–753.
- [49] E.N. Brown, N.R. Sottos, S.R. White, Fracture testing of a self-healing polymer composite, *Exp. Mech.* 42 (2002) 372–379.
- [50] E.N. Brown, S.R. White, N.R. Sottos, Microcapsule induced toughening in a self-healing polymer composite, *J. Mater. Sci.* 39 (2004) 1703–1710.
- [51] J. Rule, E.N. Brown, N.R. Sottos, S.R. White, J.S. Moore, Wax-protected catalyst microspheres for efficient self-healing materials, *Adv. Mater.* 17 (2005) 205–208.
- [52] E. Grossman, I. Gouzman, Space environment effects on polymers in low earth orbit, *Nucl. Instrum. Methods Phys. Res. B* 208 (2003) 48–57.
- [53] E.N. Brown, M.R. Kessler, N.R. Sottos, S.R. White, In Situ poly(urea-formaldehyde) microencapsulation of dicyclopentadiene, *J. Microencapsul.* 20 (2003) 719–730.
- [54] H.W. Greensmith, A.G. Thomas, Rupture of rubber. III. Determination of tear properties, *J. Polym. Sci.* 18 (1955) 189–200.
- [55] H.W. Greensmith, Rupture of rubber. IV. Tear properties of vulcanizates containing carbon black, *J. Polym. Sci.* 21 (1956) 175–187.
- [56] B.J. Blaiszik, N.R. Sottos, S.R. White, Nanocapsules for self-healing materials, *Comp. Sci. Tech.* 68 (2008) 978–986.
- [57] J.M. Kamphaus, J.D. Rule, J.S. Moore, N.R. Sottos, S.R. White, A new self-healing epoxy with tungsten (VI) chloride catalyst, *JRS Interface* 5 (2008) 95–103.